UMEÅ UNIVERSITY

Characterization of the MRI patient exposure environment and exposure assessment methods for magnetic fields in MRI scanners

Jennifer Frankel

Department of Radiation Sciences
Umeå 2021

This work is protected by the Swedish Copyright Legislation (Act 1960:729)
Project funding by the Swedish Research Council and the Cancer Research Foundation in Norrland.
Dissertation for PhD
ISBN: 978-91-7855-501-7 (print)
ISBN: 978-91-7855-502-4 (pdf)
ISSN: 0346-6612
Umeå University Medical Dissertations, New Series No 2125
Illustrations by Mattias Pierre
Electronic version available at: http://umu.diva-portal.org/
Printed by: CityPrint i Norr AB Sweden
Umeå, Sweden 2021

“The only difference between screwing around and science, is writing it down.”

Adam Savage

Table of Contents

Abstract ii

Sammanfattning på svenska iv

List of original papers vi

Other scientific contributions vii

Peer-reviewed original papers vii

Conference abstracts vii

Abbreviations viii

Introduction 1

Background 3

MRI exams 4

MRI physics 5

Coils 7

Approaching the scanner 8

Medical implants 10

Health effects 10

Various approaches to exposure assessment 13

Aim 17

Materials and Methods 18

MRI scanner 18

Experimental setup 18

Data processing 20

Suggested exposure metrics 20

MRI sequence design and protocols used 21

Magnetic field models and exposure metric proxies 22

Results 24

Exposure variability among MRI sequences 24

Exposure variability within an MRI sequence 26

Exposure assessment methods 26

Spatial field distributions 29

Discussion 32

Conclusion 41

Acknowledgements 42

References 43

Abstract

Magnetic resonance imaging (MRI) has become one of the most common imaging modalities available in modern medicine, and it is an indispensable diagnostic tool thanks to the unparalleled soft-tissue contrast and high image resolution. It is also a unique exposure environment consisting of a complex mix of magnetic fields. During an MRI scan, the patient is simultaneously exposed to a strong static magnetic field, a fast-switching gradient magnetic field, and a pulsed radiofrequency (RF) magnetic field. Transient acute effects, such as nerve excitation and tissue heating, are well known and limited by universal safety guidelines. Long-term health effects related to MRI exposure have, however, not been scientifically established, and no interaction mechanisms have been verified, despite a growing body of research on electromagnetic field exposure. Further epidemiological and experimental research on MRI exposure has been recommended but the lack of a common definition of dose or exposure metric makes evaluation of past research and the design of future experiments difficult.

The objectives of this thesis were to characterize the MRI patient exposure environment in terms of the magnetic fields involved, suggest relevant exposure metrics, and introduce exposure assessment methods suitable for epidemiological and experimental research on MRI and long-term health effects.

In Paper I, we discussed the MRI exposure environment and its complexity and gave an overview of the current scientific situation. In Paper II, we investigated the exposure variability between different MRI sequences and suggested patient-independent exposure metrics that describe different characteristics of the magnetic field exposure, including mean, peak, and threshold values. In Paper III, we presented three exposure assessment methods, specifically suited to the complex MRI exposure environment: a measurement-based method, a calculation-based method, and a proxy method.

Papers I and II showed that MRI exams are not homogenous in terms of exposure, and exposure variability exists between the individual sequences that comprise an exam. Differences in mean exposure between sequences were several-fold, peak exposure differences up to 30-fold, and differences in threshold exposure were in some cases more than 100-fold. Furthermore, within-sequence exposure variability, related to the parameter adjustments that can be made at the scanner console before the start of a scan, gave rise to 5-to-8-fold exposure increases. Paper III showed that magnetic field models could be used to approximate the exposure at arbitrary locations inside the scanner, with slight underestimation of gradient field metrics and large variability in some RF field metrics. With improvements in accuracy and efficiency, the method could become a useful

exposure assessment tool for *in vitro* and *in vivo* research as well as clinical work on medical implant safety. Our search for suitable exposure metric proxies resulted in a limited selection with low correlation between proxies and their counterpart metrics, but, with further development, the proxy method has the potential to allow for much needed exposure classification relevant to large-scale epidemiological research.

The work in this thesis has contributed to increased awareness of the unique MRI exposure environment, the characteristics of the magnetic fields involved, and the inherent exposure variability in MRI exams. The metrics and methods presented are specifically suited to exposure assessment of the unique MRI environment, and may contribute to improved research quality by allowing for meaningful comparisons between study results and for experimental conditions to be easily replicated in future studies.

Sammanfattning på svenska

Magnetisk resonanstomografi (MR), som är en av de vanligaste medicinska avbildningsmetoderna idag, är ett oumbärligt diagnostiskt verktyg tack vare den oöverträffade mjukvävnadskontrasten och höga bildupplösningen. MR-kameran är också en unik exponeringsmiljö bestående av en komplex blandning av magnetfält med olika frekvenser och fältstyrkor. Under en vanlig MR-undersökning exponeras patienten för ett starkt statiskt magnetfält på 1,5 eller 3 Tesla, ett snabbt växlande gradientmagnetfält och ett pulsat radiofrekvent (RF) magnetfält. Gradientfältet kan ibland generera en pirrande känsla i huden på armarna och benen och RF-fältet kan orsaka vävnadsuppvärmning. Dessa övergående effekter är välkända och begränsas av allmänna säkerhetsriktlinjer.

Långsiktiga hälsoeffekter relaterade till MR-exponering är dock inte vetenskapligt fastställda och det finns inga vedertagna interaktionsmekanismer. Det finns en hel del forskning på magnetfältsexponering och biologiska effekter, men resultaten är blandade och svåra att tyda. Till skillnad från joniserande strålning (används i bl.a. röntgenundersökningar), som vi vet kan skada DNA-molekylerna i våra celler och som medför en ökad risk att utveckla cancer vid alltför höga doser, så har vi inga etablerade mått på dos och exponering när det gäller låg- och radiofrekventa magnetfält. Därför kan kvaliteten på exponerings-bedömningarna skilja betydligt mellan olika forskningsstudier, vilket innebär att det är svårt att jämföra resultat från olika studier och ofta omöjligt att reproducera och verifiera tidigare forskningsresultat. Ytterligare epidemiologisk och experimentell forskning om MR-exponering behövs, men för att kunna genomföra den på ett meningsfullt sätt behövs tydliga exponeringsmått och metoder för exponeringsbedömning som är anpassade till den komplexa blandning av magnetfält som finns i MR-kameran.

Syftet med denna avhandling var att karakterisera MR-patientens exponerings-miljö med avseende på de tidsvarierande magnetfälten, föreslå lämpliga exponeringsmått och presentera exponeringsbedömningsmetoder som är relevanta för epidemiologisk och experimentell forskning om MR och långsiktiga hälsoeffekter.

I artikel I diskuterade vi MR-kamerans exponeringsmiljö och dess komplexitet och gav en översikt av det nuvarande vetenskapliga läget gällande MR och exponering. I artikel II undersökte vi hur exponeringen kan variera mellan de olika bildtagningssekvenserna som ingår i en MR-undersökning, och föreslog patient-oberoende exponeringsmått (olika typer av medelvärden, maxvärden och tröskelvärden) för att beskriva magnetfältens egenskaper. I artikel III presenterade vi tre metoder för att bedöma exponering, särskilt lämpade för den

komplexa MR-exponeringsmiljön: en metod för mätningar av magnetfälten inne i kameran, en metod som simulerar kamerans magnetfält, och en metod för att identifiera mer lättillgängliga magnetfältsrelaterade parametrar som korrelerar starkt med de egentliga exponeringsmåtten.

I artiklar I och II visade vi att MR-undersökningar inte är homogena med avseende på exponering, så det går inte att enkelt klassificera en undersökning baserat på hur länge den pågår eller vilken kroppsdel som avbildas. Exponeringen kan variera betydligt mellan de olika sekvenserna som ingår ett undersöknings-protokoll. För vissa exponeringsmått är det bara några procents skillnad mellan olika sekvenser, medan det i andra fall kan vara mer än 100-faldig skillnad i exponering. Dessutom fann vi att exponeringen för en enskild sekvens kan varieras genom att MR-kamerans inställningar justeras inför en bildtagning. Detta innebär att det finns väldig många variabler som påverkar exponeringen i en MR-undersökning, och en medvetenhet om detta är viktigt om vi ska kunna genomföra meningsfulla exponeringsbedömningar.

I artikel III visade vi hur simulerade magnetfält kan användas för att beräkna exponeringen på godtyckliga platser inuti MR-kameran. Modellen av gradient-fältet var stabil och fungerade bra för olika exponeringsmått, trots en liten underskattning av exponeringen. RF-fältets exponering visade sig vara svårare att simulera och resultaten varierade mer i jämförelsen med uppmätta värden. Med förbättringar i noggrannhet och effektivitet kan metoden bli ett användbart verktyg för exponeringsbedömning i framtida *in vitro*- och *in vivo*-studier samt i kliniska säkerhetsbedömningar, till exempel vid utvärdering av medicinska implantat. Jakten på lämpliga ersättningsparametrar för magnetfältens exponeringsmått resulterade i ett begränsat urval med relativt låg korrelation mellan parametrar och motsvarande mätvärden, så sökandet fortsätter. Med fortsatt utveckling har den här metoden potential att möjliggöra välbehövlig exponeringsklassificering som är relevant för storskalig epidemiologisk forskning.

Denna avhandling har belyst MR-kamerans unika exponeringsmiljö med fokus på de tidsvarierande magnetfältens egenskaper, och de många variabler som påverkar exponeringen under en MR-undersökning. De exponeringsmått och bedömningsmetoder som presenterats i detta arbete är särskilt lämpade för den unika exponeringsmiljö som finns i MR-kameror, och kan bidra till förbättrad forskningskvalitet genom att möjliggöra meningsfulla jämförelser mellan olika studiers resultat och upprepning av experimentella förhållanden i framtida studier.

List of original papers

This thesis is based on the following papers, which are referred to by their Roman numerals in the text. The complete papers are appended at the end of the thesis, reprinted with permission from the publishers.

I. Frankel J, Wilén J, Hansson Mild K. *Assessing exposures to magnetic resonance imaging's complex mixture of magnetic fields for in vivo, in vitro, and epidemiologic studies of health effects for staff and patients*. Front Public Health. 2018 Mar 12;6:66. doi: 10.3389/fpubh.2018.00066.

II. Frankel J, Hansson Mild K, Olsrud J, Wilén J. *EMF exposure variation among MRI sequences from pediatric examination protocols*. Bioelectromagnetics. 2019 Jan;40(1):3-15. doi: 10.1002/bem.22159.

III. Frankel J, Hansson Mild K, Olsrud J, Garpebring A, Wilén J. *Exposure assessment methods for magnetic fields in MRI*. [Manuscript]

Other scientific contributions

Scientific work by Jennifer Frankel, related to, but not included in, this thesis.

Peer-reviewed original papers

Hansson Mild K, Friberg S, **Frankel J**, Wilén J. *Exposure to the magnetic field from an induction loop pad for a hearing aid system*. Int J Occup Saf Ergon. 2017 Mar;23(1):143-145. doi: 10.1080/10803548.2016.1226597.

Wilén J, Olsrud J, **Frankel J**, Hansson Mild K. *Valid exposure protocols needed in magnetic resonance imaging genotoxic research*. Bioelectromagnetics. 2020 Apr;41(3):247-257. doi: 10.1002/bem.22257.

Conference abstracts

Frankel J, Hansson Mild K, Wilén J. *Assessment of MRI patient exposure for epidemiological studies*. Joint Meeting of the Bioelectromagnetics Society and the European BioElectromagnetics Association, BioEM2015. Asilomar, CA: The Bioelectromagnetics Society and the European Bioelectromagnetics Association; (2015). 58 p.

Frankel J, Hansson Mild K, Wilén J. *MRI patient exposure-characterization and sequence-comparisons*. The Joint Annual Meeting of the Bio-electromagnetics Society and the European BioElectromagnetics Association, BioEM2018. Piran, Portorož, Slovenia: The Bioelectromagnetics Society and the European Bioelectromagnetics Association; (2018). 420-422 p.

Abbreviations

B_0 = Main (static) magnetic field inside scanner

B_1 = Radiofrequency magnetic field

dB/dt = Gradient magnetic field time derivative

EAM = Exposure assessment method

ELF = Extremely low frequency

ELT = Exposure level tester

EMF = Electromagnetic field

FLCOM = First level controlled operating mode

FOV = Field of view

MR = Magnetic resonance

MRI = Magnetic resonance imaging

NOM = Normal operating mode

PET = Positron emission tomography

PNS = Peripheral nerve stimulation

RF = Radio frequency

SAR = Specific absorption rate (W/kg)

SGF = Switched gradient field

SLCOM = Second level controlled operating mode

Slew rate = Speed at which a gradient can be turned on and off (T/m/s)

T = Tesla

TE = Echo time

TEM = Transverse electromagnetic cell

TI = Inversion time

TR = Repetition time

T/R = Transmit and receive coil for RF field

Introduction

Magnetic resonance imaging (MRI) has become one of the most common diagnostic imaging modalities in medicine today [1]. The MRI scanner is a technological marvel capable of producing high-resolution anatomical images with unparalleled soft-tissue contrast. It is also a unique exposure environment consisting of a complex mix of magnetic fields.

During a scan the patient is exposed to three different types of electromagnetic fields (EMF) at varying strengths and frequencies. A main static field is always present, and during scanning the addition of a switched gradient field (SGF) and a pulsed radiofrequency (RF) field create the necessary conditions for image creation. In today's clinical scanners the magnetic flux density of the main field is commonly 1.5 or 3 Tesla (T), while the strength of the SGF is in the mT range, and the RF field is in the μT range [2].

Unlike adjacent imaging modalities, which rely on ionizing radiation, MRI has generally been considered innocuous, as the magnetic fields involved are found in the low-energy band of the electromagnetic spectrum. External magnetic fields induce loops of electrical current in the exposed subject, and in the frequency ranges of the SGF and RF magnetic fields in MRI such currents can cause neuroexcitation and tissue heating [3]. Such acute effects of MRI exposure are well known and limited by international safety regulations for patients [4] and personnel working near MRI scanners [5].

Long-term health effects related to MRI exposure have, however, not been scientifically established. There is a growing body of evidence supporting the theory that low-frequency magnetic fields can modify biological processes, but mixed results and the lack of an established interaction mechanism for explaining possible long-term effects, means that there is still a significant knowledge gap regarding the MRI exposure environment [6].

Further epidemiological and experimental research on MRI exposure has been recommended to close the knowledge gap and allow us to fully understand the impact of MRI on the human body [7]. Exposure assessment of magnetic fields in general is complicated [8], and an MRI scanner houses a complex mix of magnetic field strengths and frequencies, making it a difficult exposure environment to analyze. The lack of a common definition of dose or exposure metric makes evaluation of past research and design of future experiments challenging [9].

The empirical work in this thesis focuses on the unique exposure environment inside an MRI scanner and the characteristics of the magnetic fields experienced during a scan. The aim is to improve our understanding of the MRI exposure environment and provide relevant metrics and assessment methods suitable for future epidemiological and experimental research on MRI and long-term health effects.

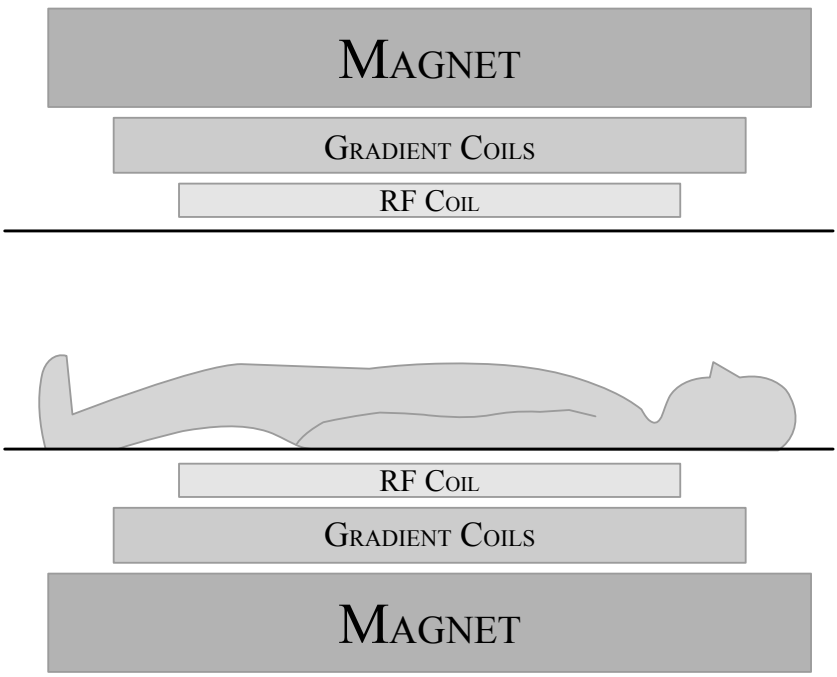

Figure 1. Schematic drawing of the coils inside a cylindrical MRI scanner and their positions around the scanner bore.

Background

Much has happened since Nobel laureate Paul Lauterbur's groundbreaking 1973 Nature publication, in which he introduced the addition of a magnetic field gradient to produce anatomical magnetic resonance (MR) images with spatial resolution [10]. MRI has grown to become one of the most utilized diagnostic imaging modalities available in modern medicine, with more than 33 000 MRI scanners worldwide [1]. The soft-tissue contrast and resolution are unparalleled, and MRI is uniquely versatile, as it can be employed for functional as well as anatomical imaging [11].

Early clinical scanners had static fields with magnetic flux densities of 0.15 Tesla (T), and high field systems with 1.5 T were introduced by General Electric in the mid 1980s [11]. Clinical scanners today are high-field systems, and typical amplitudes are 1.5 or 3 T, with a steep drop-off outside the scanner opening so that the magnetic flux density drops to single-digit mT a few steps away from the scanner table. The most common MR scanner configuration is the closed bore cylindrical system shaped like a big tunnel into which the patient is transported for imaging [11]. The main field is created with a superconducting electromagnet consisting of solenoidal coils around the bore of the scanner. Liquid helium cools the magnet down to 4 °Kelvin (-269 °Celsius) to eliminate resistance to the strong current flowing through the coils.

Inside the main magnet are the gradient coils, which are also wrapped around the bore of the scanner (Figure 1). These coils produce a temporally and spatially varying magnetic field which adds linear gradients to the static field. The SGF changes at a rate of several kHz and the performance of a scanner gradient coil system is usually described in terms of maximum amplitude and slew rate, which is the speed at which a gradient is turned on and off. Technological advances over the years have led to current MRI systems with amplitudes up to 80 mT/m and switching slew rates of up to 200 T/s/m [1].

The innermost coil structure is the RF body coil (Figure 1), which is located closest to the scanner's inner bore wall. It produces a circularly polarized magnetic field (Figure 2), applied in short bursts, or pulses, with a carrier frequency in the MHz range. The pulses can have different shapes, or "envelopes", depending on the design of the RF field, and peak pulse amplitudes can be as high as 50 μT [1].

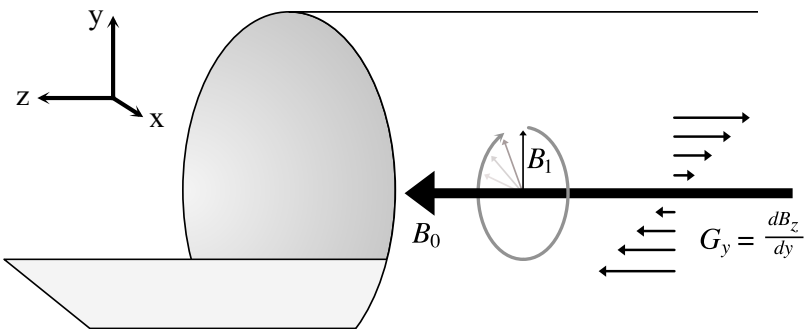

Figure 2. Image-producing magnetic fields inside a cylindrical MRI scanner. The main magnetic field, B_0, is directed along the z-axis of the scanner. The gradient field is shown here as a gradient along the y-axis, $G_y = dB_z/dy$. The RF field, B_1, is rotating in the transverse plane.

The magnetic fields produced in an MRI scanner are found in the low-energy band of the electromagnetic spectrum, at frequencies that are lower than for ultraviolet radiation and visible light. Magnetic fields in the kHz - MHz frequency range are categorized as non-ionizing radiation because they do not have enough energy to ionize atoms with which they interact, i.e., they cannot fully remove an electron from an atom upon collision. Ionizing radiation is found at higher frequencies of the spectrum, e.g., X-rays and gamma-rays. In this thesis the term electromagnetic field (EMF) is used in reference to the range of frequencies involved in MRI, including the static (0 Hz), SGF (kHz), and RF (MHz) magnetic fields.

MRI exams

A clinical MRI exam can last anywhere from a few minutes to more than an hour, and a typical exam protocol is built up of multiple MRI sequences, each lasting somewhere between a few seconds and several minutes. Each sequence is designed with a particular imaging purpose in mind, e.g., to clearly show fat vs. water contrast or to provide exceptionally high-resolution detail [12]. Different types of images of the same anatomical region can be diagnostically useful, but since each additional sequence adds to the total time the patient has to spend in the scanner, sequences are chosen carefully to maximize the amount of relevant information while limiting the necessary total scan time.

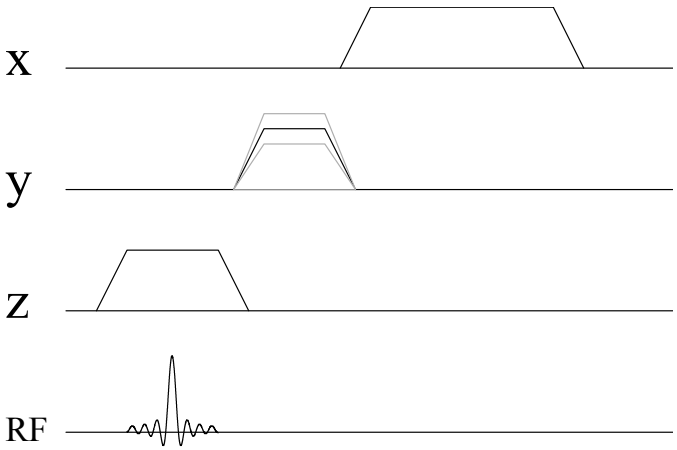

Figure 3. Example of a pulse sequence diagram. The top three panels show the waveforms produced by each of the gradient coils and the bottom panel shows an RF pulse. During an MRI scan this pulse sequence segment is repeated many times with varying amplitudes on the phase-encoding gradient (y-panel).

An MRI pulse sequence is a pre-programmed set of gradient and RF field waveforms, sometimes illustrated by a sequence diagram showing the timing and amplitude of the waveforms for each gradient coil and the RF pulses (Figure 3). Certain features of the scan are fixed, decided in the original pulse sequence design, but many parameters are variable and can be adjusted at the scanner console before a scan. The size of the area included in the image is decided by parameters such as field of view (FOV), slice thickness, and slice spacing. Adjustable timing variables include repetition time (TR), echo time (TE), and inversion time (TI), which determine how the gradients and RF pulses are spaced over time in the sequence.

MRI physics

A brief look at what happens on a subatomic level is helpful when discussing MRI and the magnetic field exposure involved. The hydrogen nucleus, ^{1}H, which consists of a single proton, is abundant in the human body as it is a major component of both water and fat. Protons belong to a class of particles which have the quantum mechanical property of *spin*, a form of angular momentum not produced by rotation but an *intrinsic* property of the particle itself. Particles with nonzero spin have a magnetic moment and experience a torque when placed in an external magnetic field, causing them to precess around the direction of the field at a specific frequency (Figure 4). The resonance frequency of a particle is proportional to the strength of the magnetic field, and protons, often referred to as “spins” in the context of MRI, have a gyromagnetic ratio of 42.577 MHz/T. This

interaction between spins and magnetic fields is the phenomenon upon which MRI technology is based, and for a more in-depth description of the properties of spin particles the reader is referred to Malcolm H Levitt's book on spin dynamics [13].

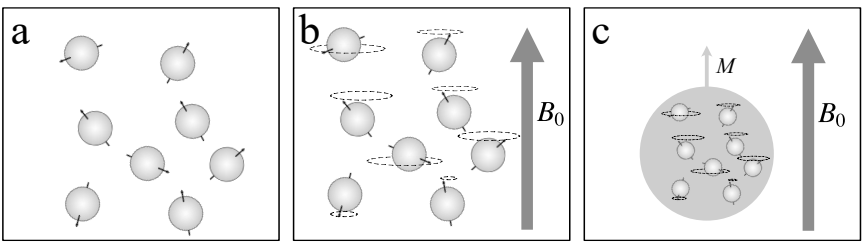

Figure 4. Spin particles (hydrogen nuclei) (a) without an external magnetic field present (isotropic distribution of spin orientations), (b) with an external magnetic field present (all spins are precessing around the direction of the magnetic field, B_0), and (c) shown as a uniform group with a common net magnetization vector M.

The distribution of spin orientations is isotropic without an external magnetic field, but when one is applied, there is a slight bias towards spin orientations with magnetic moments parallel to the magnetic field. This means that, even though individual spin magnetic moments can point in any direction, a large group of precessing protons produce a net magnetization along the external field. This net magnetization is tiny compared with the static field of an MRI scanner, and unmeasurable when aligned with the B_0. However, the addition of a perpendicular magnetic field which rotates around the static field axis at resonance frequency, is experienced by the spins (inside their rotating frame of reference) simply as a slight alteration to the direction of the total external magnetic field. This results in rotation of the net magnetization away from the B_0 axis, towards the transverse plane. This is the purpose of the RF magnetic field – to "flip" the net magnetization a number of degrees (the flip angle) away from the static field axis. The now rotating net magnetization gives off a weak, but measurable, RF magnetic field in the transverse plane, with a signal strength proportional to the amount of hydrogen present in the sample. This is the MR signal which is subsequently translated into an anatomical image of the different structures and tissue types inside the body.

Spatial encoding is provided by the SGF, which momentarily adds to, or subtracts from, the main field strength so that different regions in the imaged slice correspond to slightly different resonance frequencies. In a 3T scanner the resonance frequency is 127.7 MHz at the isocenter and varies by a few kHz across the chosen field of view when a gradient is applied. An image slice is selected by the application of a slice-selection gradient along the appropriate axis (e.g., the z-

axis for axial image slices, as shown in Figure 3) together with an RF pulse with a frequency range matching that of the spins within the desired slice thickness. The slice is then effectively divided into a two-dimensional coordinate system of pixels, with each pixel-location corresponding to a unique frequency. This frequency grid is created by applying gradients along each of the two remaining axes. First a phase-encoding gradient is applied along one axis (the y-axis in Figure 3) to introduce a spatial position-encoding phase-variation that persists even after the gradient has been turned off. Then a frequency-encoding gradient is applied along the other axis (the x-axis in Figure 3) to introduce a frequency variation along that axis. This procedure is repeated with different strengths of phase-encoding gradients to cover a range of phase- and frequency combinations. The RF pulse is applied together with the slice-selection gradient once for every phase-encoding step, to flip the net magnetization (shown in Figure 4 c) of the spins away from the axis of the main field. The resulting MR signals can then be decoded so that signal frequency components are translated into image pixel locations.

The physics described here is specifically related to the exposure aspect of MRI. For more in-depth descriptions of the image-creating aspects of MRI the reader is referred to more comprehensive textbooks on the subject, such as MRI From Picture to Proton by McRobbie et al. [11] and Handbook of MRI Pulse Sequences by Bernstein et al. [12].

Coils

The magnetic fields required to create resonance-precessing protons and flipped net magnetizations are created by the movement of electrical current through coils. Current flow through a wire will cause circular magnetic field lines around the wire (think of the right-hand grip rule), and with two wires the magnetic field strength can be increased, or, if the current flows are in opposite directions, the magnetic fields from the wires can cancel each other out. A magnetic field of desired magnitude and direction can thus be designed by running current through specifically configured coil wires, and one arrangement that can produce a nearly uniform magnetic field inside the structure is the Helmholtz coil which consists of two circular loops of radius a, placed a distance a apart [14].

In a typical cylindrical MRI system, the three gradient coils are positioned around the scanner bore. The z-gradient is usually produced with circular hoops based on the Helmholtz coil structure, while the x- and y-gradient coils are usually both based on a saddle coil configuration, identical in design but with one coil rotated 90 degrees around the cylinder axis with respect to the other coil [15]. The goal when designing a gradient coil system is to produce linear gradients within a large enough imaging volume, so desired amplitudes and slew rates can be reached

without causing discomfort to the patient and with a minimum amount of image distortion [16].

The purpose of the SGF is to gradually add to or subtract slightly from the magnitude of the strong static field across a plane, to produce a highly specific geometric grid of varying spin frequencies in the imaged tissue. Therefore, in order to match the direction of the static field, the gradient coil system is designed to produce a z-directed field, B_z, which can vary in strength along any axis. This is accomplished by three separate coils with independent power amplifiers, and each coil produces a gradient, G, along one of the scanner's main axes X (right-left), Y (up-down), and Z (in-out). So, while the gradients extend along the Cartesian axes of the scanner, the image-producing B-fields created by each coil are all axially directed such that

$$G_x = \frac{dB_z}{dx}, G_y = \frac{dB_z}{dy}, G_z = \frac{dB_z}{dz} \quad (1)$$

In addition to the desired B_z field, each gradient coil also produces concomitant fields B_x and B_y in accordance with Maxwell's equations [17]. These gradient field components are orthogonal to the intended image-producing field, so they can cause distortions that need to be corrected in the imaging process. However, with current clinical systems of 1.5 or 3 T and maximum gradient strengths of 40-50 mT/m, the total impact of the concomitant fields on image quality is small, sometimes even negligible, depending on coil design and sequence type [18].

The RF field differs from the SGF in many ways. While the SGF is a combination of magnetic fields produced by three separate orthogonal coils, the RF field is produced by a single transmit coil, however, that coil can take many forms [19]. In the cylindrical scanner system, there is usually a transmit coil built into the scanner, called a body coil, shaped like a birdcage around the scanner bore. There are also separate RF coils that can be used locally, for example head coils and surface coils with transmit and receive (T/R) functionality.

The RF transmit coil is designed to provide a homogenous circularly polarized B_1 field in the imaging volume [16], inside the scanner bore in the case of a T/R body coil, or more locally in the case of a separate T/R coil. The B_1 field rotates in the xy-plane, perpendicular to the static B_0 field, in order to flip the spin net magnetization away from the z-axis.

Approaching the scanner

One of the first things you may notice as you approach an MRI scanner is a pulling force due to the static magnetic field. If you happen to be wearing something

ferromagnetic, such as a pair of metal-framed glasses, you feel a slight tug towards the scanner. The static magnetic field, which is several Tesla strong, can make lethal projectiles out of ferromagnetic items, and patients who are about to be scanned should of course not be wearing anything metallic. Safety protocols should be in place at every MRI scanner to ensure that nothing unsafe enters the room as accidents involving non-MRI-safe items near the scanner pose the greatest safety risk to MRI patients and personnel [1].

Also, the scanner room is a bit noisy, with the constant chugging of the cryogenic pump keeping the superconducting magnet stable and the buzzing of fans ensuring continuous air circulation in the scanner. However, the real racket starts once the scanning begins. Rapidly changing gradient coil currents, in the presence of B_0, produce significant Lorentz forces that act upon the gradient coil windings [20]. This causes vibrational motion of the coils in a frequency range that results in acoustic noise – a loud knocking sound. Anyone in the room during this time must wear proper ear protection to prevent auditory damage.

Apart from the safety hazard of projectiles and loud noises, one can also experience a range of physical symptoms simply by moving through the strong static field near the scanner. Symptoms reported by staff working near MRI scanners include vertigo, nausea, drowsiness, headaches, memory loss, sleep disorders, illusions of movement, and difficulties concentrating [21-26]. For patients such symptoms are mainly experienced before or after scanning, while moving into or out of the scanner, whereas the actual exam does not involve any movement through the static field. Hansson et al. [27] reported that dizziness was the most frequently experienced short-term effect among study participants during examinations in a 7T scanner, especially while moving into and out of the magnet. Such transient symptoms are less noticeable at clinical field strengths of 1.5 and 3 T.

With the patient safely positioned in the scanner, the technician controls the scanning process from the console outside the scanner room. Patient data such as height and weight are recorded, and a relevant scan protocol is chosen. Every exam starts with a quick localizer sequence that produces a low-resolution image used for planning. Slice position is determined based on the localizer image, and before each scan sequence is initiated, it is possible to adjust various sequence parameters, e.g., field of view and slice thickness, to tailor the scan to the individual patient. Every imaging sequence starts with a prescan, which is an automated process where the scanner performs multiple calibrations to optimize performance [2]. The prescan process includes coil tuning, center frequency modifications, and RF transmitter and receiver gain adjustments. The RF coil system is calibrated to the individual patient since, for example, the exact amount

of RF power needed to generate a known flip angle depends both on the type of transmitter coil but also on the weight of the patient [11].

The static magnetic field is permanently present in an MRI scanner, regardless of whether any exam is underway. The low-frequency SGF and the pulsed RF fields, however, are only added during active scanning. Magnetic fields induce electric currents in conductive material, including the human body, and the internally induced electric field is related to the time rate of change of the flux density of the magnetic field [3]. Depending on the frequency, induced electric currents can cause various physiological effects in the body of the scanned subject.

Medical implants

Scanning patients with medical implants introduces an additional source of risk to patient safety as well as image quality, and each implant must be carefully evaluated to determine whether it can be allowed into the scanner. Passive devices, such as, e.g., joint replacements, stents, and aneurysm clips, are implanted within the patient but do not use electrical power. Risks from scanning passive implants include movement or displacement of the device, heating, and induction of electrical currents [1]. Active devices, such as cardiac pacemakers and cochlear implants, involve electrically powered mechanisms that risk malfunctioning when exposed to strong magnetic fields. While historically banned from the MRI environment as “MR unsafe”, some active implants can now be labeled “MR conditional” and allowed into the scanner given compliance with certain conditions, e.g., limits on total scan time or on RF and SGF intensity, or restrictions on the anatomical location of the scan [1]. The challenge is to determine what level of exposure is safe for each individual implanted device, so as not to expose anyone to undue risk, but also not to withhold an important medical exam from anyone due to unwarranted overcautiousness.

Health effects

The SGF switches at frequencies in the kHz range which matches the physiological firing frequency of neurons so that a possible immediate effect of exposure to the SGF is peripheral nerve stimulation (PNS). This occurs if the time derivative of the SGF, dB/dt, is sufficiently large and the effective exposure time is long enough [28]. Mild PNS is experienced as a tingling sensation or sometimes light muscle twitching. More intense PNS, caused by higher dB/dt levels extending for longer periods of time, is experienced as discomfort or even pain [29].

The RF field, which oscillates at a much higher frequency than the SGF, causes heat absorption in the scanned tissue. Excessive tissue heating during an MRI scan is avoided by limiting the RF-field specific absorption rate (SAR), measured in W/kg. SAR describes the rate of energy absorption per unit mass by the scanned tissue, and it is usually expressed as a time-averaged value, so it limits the average amount of energy absorbed over a specific period of time.

All clinical MRI scanners have two different safety modes controlling the SGF and RF exposure, to limit discomfort and prevent acute harm to patients: normal operating mode (NOM) and first level controlled operating mode (FLCOM). These two modes provide explicit limits for SAR and dB/dt during scanning so that the acute effects of tissue heating and PNS are kept within a safe range [4]. A whole-body SAR value of 2 W/kg is allowed in NOM and 4 W/kg in FLCOM, and partial body SAR values of up to 10 W/kg can be accepted for exposure to limited parts of the body. There is also a second level controlled operating mode (SLCOM), where SAR > 4 W/kg is allowed, and that carries a significant risk of discomfort for the patient. Use of this mode is only relevant for research studies, and its use requires explicit ethical approval.

While the dB/dt limit is the same for all MRI sequences, given a specific scanner operating mode, the scanner-provided SAR value is sequence-specific. For each MRI sequence the scanner estimates a six-minute time-averaged whole-body SAR value, based on the applied RF field and the weight of the patient. There is no universal standard for estimating SAR, so each MRI scanner manufacturer has its own proprietary method for doing so. The scanner-provided SAR value of a sequence can include a significant safety margin which was illustrated by El-Sharkawy et al. [30] with independent B_1 measurements showing an overestimation of the scanner-provided body-average SAR as compared with the actual power deposited.

Even though MRI technology has been around for more than 40 years, the question of whether it can cause long-term health effects has yet to be definitively answered. The magnetic fields used in MRI belong to the low-frequency band of the electromagnetic spectrum, and the International Commission on Non-Ionizing Radiation Protection (ICNIRP) has established guidelines for limiting occupational and general public exposure to electromagnetic fields of frequencies up to 300 GHz [31, 32]. Patients in need of medical treatment temporarily land outside the two categories of occupational and general-public exposure limited by ICNIRP's guidelines. When the benefits of a diagnostic procedure or medical treatment outweigh the inherent risks, we can accept higher levels of exposure than we otherwise would. Therefore, there are special exposure guidelines for medical equipment. The European Committee for Electrotechnical Standardization (CENELEC) has issued a safety standard on medial electrical

equipment, dictating safety limits for exposure to magnetic fields in MRI scanners, and all EU member states are bound to comply with the stipulated regulations [4]. These limits on SGF and RF exposure are solely based on knowledge about acute effects, as are the general guidelines for limiting occupational and general public exposure to electromagnetic fields. Despite a long history of research on electromagnetic field exposure, there is currently no well-established scientific evidence of long-term health effects [6].

Epidemiological research, dating as far back as the 1970s, has shown a link between exposure to extremely low frequency (ELF) magnetic fields and childhood leukemia [33-35], with the aggregated result showing an association between long-term exposure to ELF magnetic fields above 0.4 μT (year-average) and an increased risk of developing pediatric leukemia. More recently, a large record-based case-control study of childhood leukemia in California, USA showed a small excess risk in the highest exposure group, consistent with previous findings [36]. Exposure to RF magnetic fields has become increasingly relevant with the growing use of RF-based communications technology. Epidemiological research on an association between RF exposure and cancer has been conducted in several large studies on mobile phone use [37-39]. No epidemiological studies investigating cancer incidence in MRI patients or personnel have yet been undertaken, although some other endpoints have been studied in relation to repeated or long-term MRI exposure, such as, e.g., neurocognitive function [40], accident risk [41], abnormal uterine bleeding [42], development of hypertension [43], and sleep quality [44].

There is a knowledge gap regarding the interaction between low-frequency magnetic fields and biological tissue, and a number of mechanisms have been suggested, although none has been firmly established and demonstrated in humans [6]. Oxidative stress due to the free-radical pair mechanism has been suggested as one of the more plausible explanations for effects of exposure to low-intensity RF fields at frequencies below 150 MHz [45], and adaptive responses allowing the exposed system to repair the damage during a recovery period have been suggested as an explanation for some of the variations in study results over the years [46]. Low-frequency exposure-studies which show varying levels of impact on cell activity depending on the spatial coherence of the applied magnetic field, such as that of Litovitz et al. [47], suggest that the exact format of the exposure matters greatly, and small variations in applied exposure will produce very different results. Again, this may explain some of the difficulties we, as a research community, have had in identifying and verifying interaction mechanisms between low-intensity magnetic fields and biological tissue. Elusive effects are difficult to repeat when our metrics and methods for exposure assessment are too blunt [48].

In the past two decades, several *in vivo* and *in vitro* studies on MRI exposure and genotoxicity have been performed, and they have tried to answer the specific question of whether MRI exams can cause DNA damage. However, the results are inconclusive. Some research groups have found indications of increased DNA damage in connection with MRI exposure [49-53], while others have not [54-58]. The mixed results are difficult to evaluate, partly due to the lack of proper exposure assessment, as we discussed in our recent publication [59].

The International Agency for Research on Cancer (IARC) classifies exposure agents in terms of carcinogenicity, i.e., the likelihood of exposure resulting in the long-term health effect of cancer. Classifications are based on the currently available research on each exposure agent, and for something to be classified as Group 1: "carcinogenic to humans" a significant amount of scientific evidence is required. A clear connection between exposure and effect must be shown, usually through epidemiological research, and an explanation for the effect must be established through experimental research on the interaction mechanisms between the exposure agent and the human tissue. RF and extremely low frequency (ELF) electromagnetic fields, which includes the range of frequencies found in MRI scanners, have been classified by IARC as Group 2B: "possibly carcinogenic to humans" [60, 61].

Various approaches to exposure assessment

In 2015 the Scientific Committee on Emerging and Newly Identified Health Risks (SCENIHR) published an updated scientific opinion on the current state of research on health effects from exposure to electromagnetic fields [7]. Based on comprehensive evaluations of existing research they made a number of recommendations, including calls for cohort studies into the effects of MRI exposure and *in vivo* studies investigating genotoxic effects following MRI investigations. If done correctly, such research could provide important pieces of the puzzle, but that requires comprehensive exposure assessment which has not always been applied in past research.

There is a definite knowledge gap regarding the MRI exposure environment, and to fill this gap we need epidemiological research to show whether there are long-term health effects, and we need experimental research to explain the interaction mechanisms between the magnetic fields and the biological tissue [62]. However, research involving exposure assessment of electromagnetic fields (EMF) is a complicated area of study [8]. Exposure is defined as the contact between a substance or agent and a surface of the human body [63]. In chemical toxicology, dose typically refers to the amount of a chemical substance given to a subject, expressed as mass units per body weight or surface area. Ionizing radiation, used in radiotherapy and medical imaging, is measured in the physical unit Gray (Gy),

which describes the absorbed dose and is defined as the amount of energy absorbed per kilogram of matter (J/kg). A corresponding definition of dose does not exist for low-frequency EMFs, and Hansson Mild and Mattsson [9] discussed the difficulty in determining possible health risks associated with exposure to EMFs when there is no agreed upon dose-description. Because of the complexity in how electromagnetic fields interact with the human body, including individual physiology-dependent factors, most epidemiologists refer to the unperturbed EMFs rather than the internal induced fields, and use various proxies to describe the complex exposure [63].

In the ICNIRP guidelines on limiting exposure to low-frequency electromagnetic fields, basic restrictions for human exposure to magnetic fields are expressed in terms of internal electric field strength (V/m), and corresponding reference levels for the external magnetic field are provided in terms of magnetic field strength, H (A/m) and magnetic flux density, B (T) [31]. For RF fields the basic restrictions are expressed in terms of whole-body average (or local head/torso or limb) SAR (W/kg) and the corresponding reference levels are expressed in terms of incident H-field strength, H (A/m) or incident power density, S (W/m^2) [32].

For medical implant safety assessment, SAR is often used to describe the RF exposure limit [64], and MRI scanners are required to provide a predicted SAR value for each sequence. Recently, B_{1RMS} was introduced as an additional RF field metric in the MRI safety standard, so now scanner manufacturers are required to provide that as well [4]. $B1_{RMS}$ is the root-mean-square (RMS) of the RF field, B_1, averaged over any 10 s period of the scan and estimated at the RF transmit coil center. It is a patient-independent metric, and it is calculated in the same way on all MR systems, so it is a more uniform way of describing the RF exposure than with SAR and thereby arguably a better parameter to use as an implant scan condition [1]. Regarding SGF exposure, most active implanted medical devices have a slew rate condition, expressed in terms of T/m/s, or, in some cases, expressed as a dB/dt limit (T/s) [1]. Risk assessments can be performed by comparing the maximum slew rate of the scanner to the one tolerated by the device in question, but that is quite a blunt assessment approach, so Trevisan et al. [65] proposed a method for sequence-specific slew rate evaluation, involving gradient coil voltage measurements and calculation of frequency-encoding gradient plateau values.

Internal electric fields, caused by exposure to external magnetic fields, are difficult to measure in humans, so numerical simulations of gradient- and RF-induced fields can provide valuable dosimetric information [66]. There is a growing virtual human population of detailed anatomical models, which take into account the inhomogeneity of internal structures and tissues of the human body [64]. With analytical or numerical models of the MRI-related electromagnetic

fields, internal effects such as, e.g., whole-body and local RF absorption (W/kg) [67] and gradient field-induced heating of metallic implants (°C) [68] can be estimated in humans for various conditions.

In many of the *in vitro* and *in vivo* studies on MRI and genotoxicity performed over the past 20 years, descriptions of SGF and RF exposure conditions were quite limited [59]. Scanner-estimated SAR values were often used to define the RF exposure. In their study on cardiac MRI and micronuclei induction, Simi et al. [49] presented the RF exposure in terms of total energy absorbed by the human subject (J), defined as a sum of the SAR values for each sequence weighted by the relative sequence repetition time, multiplied by the human subject mass. Maximum gradient coil output, in terms of strength (mT/m) and speed (T/m/s), of the scanner in question, were used to describe SGF exposure in several studies [49, 51-53, 57, 58, 69, 70]. In other cases, the maximum gradient strength (mT/m) and slew rate (mT/m/ms) achieved during a specific MRI sequence were provided [55, 56].

Large epidemiological studies cannot rely on complex patient-dependent parameters such as induced current density or SAR, but still need metrics that describe the exposure, and often use proxy metrics that describe the exposure environment without the patient in it [63]. In past case-control studies investigating an association between ELF magnetic field exposure and childhood leukemia, exposure classifications were based on such things as residential proximity to power lines, measurements of magnetic fields within residences or through personal monitoring, and residential power line wiring configurations [36]. In epidemiological studies on cell phone use, RF exposure classifications have been based on estimated level of usage, measured in hours of cumulative use, either self-reported or based on subscription data [38]. Attempts at defining exposure in terms of energy deposition (J/kg) include a combination of the phone usage time with weighting factors based on the different levels of power output from different types of phones [71], and calculations of specific absorption per day (SAD) and specific absorption per phone call (SAC) based on phantom E-field measurements for different phone types [72]. Inyang et al. [73] discussed the difficulties in assessing exposure from mobile phone use due to issues like recall bias which can lead to misclassification, and suggested the use of hardware modified phones for more accurate exposure assessment of RF radiation.

Occupational exposure to MRI-related magnetic fields is an area of research where the task of exposure classification has been handled in a variety of ways. Wilén and de Vocht [21] classified exposure in terms of time spent in the MRI examination room (average number of minutes per day) and the strength of the static magnetic field. Job title was used to classify workers at an MRI device manufacturing facility into groups of high (> 4 h/week), low (< 4 h/week) or no

exposure to the static magnetic field experienced in the vicinity of MRI systems [43]. Hansson Mild et al. [74] have suggested that, rather than use of job title as a proxy for exposure, exposure categories should be defined based on the different types of magnetic fields included in the total exposure – just the static field or combinations of the static field, SGF and RF field. Huss et al. [42] applied this approach when differentiating between radiographers working in the MRI scanner room under different circumstances: often, sometimes, or never, during image acquisition.

EMF exposure has been studied for some time, and there have been many different approaches to dosimetry and exposure classification, some more difficult to evaluate than others. To close the knowledge gap that still exists regarding MRI and long-term health effects we need large-scale population-based research and cellular-level experimental studies [7, 62]. In both cases it is important that the exposure assessment is clear and precise, so that experimental conditions can be replicated, and research findings can be compared between studies. The EMFs in MRI are complex, with temporal and spatial variations, which make it difficult to characterize the exposure in simple terms. Highly specific descriptions detailing every aspect of the exposure involved may be relevant in small prospective *in vitro* studies, while large retrospective epidemiological studies require exposure proxies which allow for a more general exposure classification. In both cases, however, it is vital that assessment and classification are based on the actual exposure. The metrics chosen to describe the exposure must reflect true characteristics of the exposure environment so that specific hypotheses about cause and effect can be properly tested.

Aim

The overall aim of this thesis was to increase our understanding of the complex MRI environment from an exposure perspective. Specifically, the objectives were to describe the MRI patient exposure environment in terms of magnetic field characteristics (Paper I), investigate exposure variability in clinical MRI exams for the purpose of exposure classification (Paper II), and develop exposure assessment methods specifically suited to epidemiological and experimental research on MRI (Paper III).

Materials and Methods

The empirical work in this thesis revolved around measurements of the magnetic fields found inside an MRI scanner. The SGF and RF magnetic fields were measured during active MRI scans, and the data from such measurements were analyzed to give us a better idea of what the exposure looks like and to allow for the extraction of exposure metrics.

In Paper I we discussed the MRI exposure environment and its complexity. We gave an overview of the current scientific situation, noting the lack of discussion in the literature about combinations of multiple types of exposure such as are found in MRI and the lack of suitable exposure metrics and exposure assessment methods for studying MRI and long-term health effects.

In Paper II we investigated the exposure variability between different MRI sequences, and the possibility for variability within a single sequence. We measured the SGF and RF fields during scanning of several clinical MRI sequences and suggested a set of patient-independent exposure metrics that describe different characteristics of the magnetic field exposure.

In Paper III we presented different exposure assessment methods specifically suited to the complex MRI exposure environment. Three approaches were described: a measurement-based method, a calculation-based method, and a proxy-method. The goal was to contribute MRI-specific exposure assessment methods to allow for meaningful comparisons between study results and for experimental conditions to be easily replicated in future research studies.

MRI scanner

Magnetic field measurements were performed inside the bore of an integrated, 3T SIGNA PET/MRI system (GE Healthcare, Chicago, IL). The scanner includes a positron emission tomography (PET) unit, however, only MRI functionality was utilized for the work in this thesis. Measurements were taken of the magnetic fields generated by the gradient coil system and the built-in RF body coil. No separate RF transmit/receive coils were investigated, but for some measurements a receive-only RF head coil was included in the setup, and for all measurements water-based phantoms were used to provide an MR-signal.

Experimental setup

The experimental setup for measurements of magnetic fields inside the MRI scanner is shown in Figure 5. As detailed in Papers II and III, we used a commercial exposure level tester (Narda ELT-400, Narda Safey Test Solutions,

Pfullingen, Germany) with a three-dimensional probe and a modified extension cable for SGF measurements. The probe contains orthogonal pickup-coils which measure the changing field, dB/dt, in three directions simultaneously. The signals are then integrated by the ELT, which outputs the gradient field, B, for each direction. Lacking an equivalent commercial option for RF measurements, we used a one-dimensional pickup-coil, made in-house, to measure the RF B_1 field. This meant that we could only measure B_1 in one direction at a time. The conversion between measured voltage signal and the actual RF magnetic field was calculated from calibration measurements done with the coil and cable inside a transverse electromagnetic (TEM) cell with known magnetic field strengths in the appropriate frequency range.

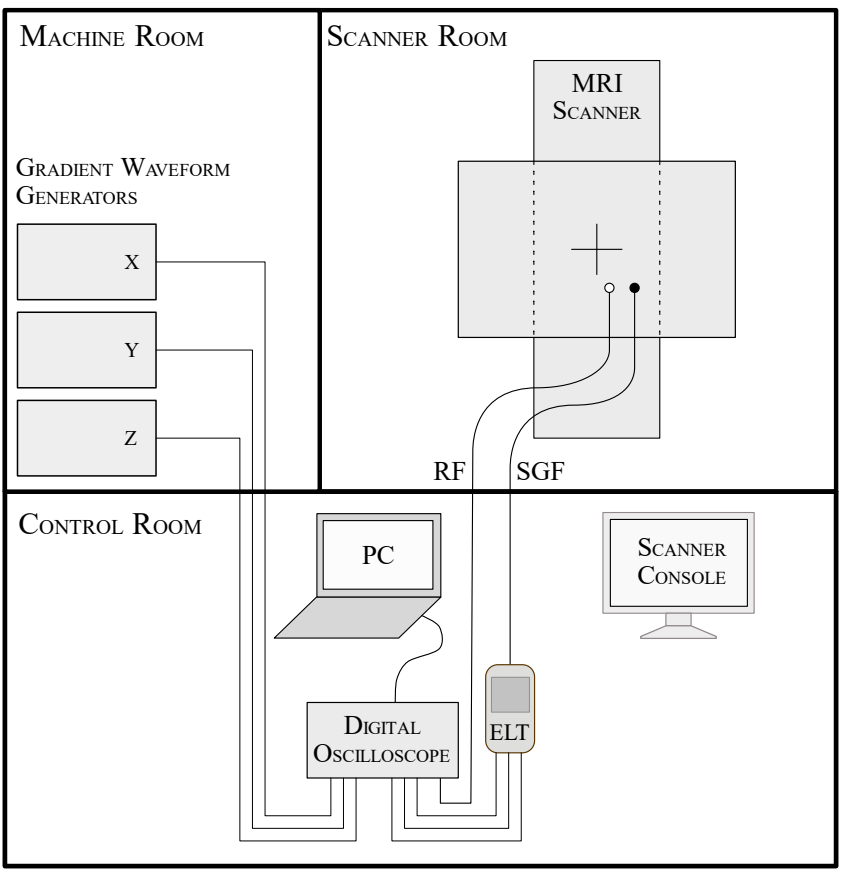

Figure 5. Schematic of the experimental setup (not to scale). SGF and RF magnetic field signals were measured with induction coils inside the scanner, and gradient coil control signals were acquired from the waveform generators in the machine room. All signals were collected through a digital oscilloscope connected to a PC laptop in the control room.

Data processing

All measured signals were captured via a digital oscilloscope connected to a laptop, and subsequent data processing and analyses were performed in Matlab. The total gradient magnetic field, $B_{tot}(t)$, was calculated from the three measured gradient field components $B_x(t)$, $B_y(t)$, and $B_z(t)$ as

$$B_{tot}(t) = \sqrt{\left(B_x(t)\right)^2 + \left(B_y(t)\right)^2 + \left(B_z(t)\right)^2} \quad (2)$$

since the SGF exposure at any point in space and time is the resultant/vector sum of all three components. $B_{tot}(t)$ was analyzed for peak and plateau amplitudes and steepness of rising and falling slopes as detailed in Paper II.

As three-dimensional RF field measurements were not available, the total RF field was represented by one-dimensional x- or y-directed measurements of $B_1(t)$. The signal picked up by the induction coil was the time-derivative of the RF field, $dB_1(t)/dt$, but since the carrier signal of the pulsed RF field is an amplitude-modulated sine curve $dB_1(t)/dt$ could be used as an approximation of the $B_1(t)$ signal. Furthermore, the RF field was assumed to have identical x- and y-components and a minimal or nonexistent z-component. In Paper III this assumption of symmetry was investigated by matching up RF signals from three orthogonal measurements. In Papers II and III $B_1(t)$ was analyzed for pulse amplitudes, widths, and temporal spacing within the sequence.

Suggested exposure metrics

In Papers II and III we suggested metrics suitable for exposure assessment of the MRI environment, as they can be used to objectively characterize the exposure environment. They are all based on measurements of the SGF and RF magnetic fields and include three types of metrics: mean values, peak values, and threshold values. These exposure metrics are based on magnetic field characteristics rather than internal effects in the exposed subject, so they are patient independent.

Some RF field mean value metrics suggested were B_{1RMS} for an entire sequence (μT), B_{1RMS} for a single pulse (μT), and B_1 mean pulse height (μT). SGF mean value metrics included B RMS (mT) and dB/dt mean (T/s). Peak metrics included B_1 maximum pulse height (μT), B peak (mT), and dB/dt peak (T/s). Examples of threshold values were B_1 duty cycle (%) and portion of sequence (s) with dB/dt > 10 T/s.

Several different metrics were suggested because different types of metrics inform us about different aspects of the exposure. We provided a selection and there are surely additional ones that could be of interest. It is, however, beyond the scope of this thesis to determine which ones are the most significant from a biological point of view. The ultimate choice of which metric(s) to use in any study must be based on the hypothesis about the biological mechanisms involved.

MRI sequence design and protocols used

A special MRI sequence was designed for the method development in Paper III. The sequence contained a long series of x-, y-, z-gradients in different combinations which allowed us to measure the gradient B-field components produced by each of the scanner's three gradient coils at different locations inside the scanner. The sequence included single gradients (alone) on each of the coils, combinations of two gradients simultaneously (xy, xz, and yz), and finally a triple gradient with all three coils active at the same time (Figure 6).

In Paper II a brain scan protocol consisting of seven different imaging sequences was investigated for exposure variability. Different sequence types were included, e.g., 2D and 3D, spin echo and gradient echo, T1-weighted and T2-weighted, diffusion-weighted, vascular, etc. The set was considered a representative selection of sequences from the most common brain scan protocols implemented at the radiology department of a major Swedish children's hospital. In Paper III a brain scan protocol consisting of six different imaging sequences was used to evaluate exposure assessment methods. This was the standard adult brain scan protocol used at our local radiology department, and it also included a variety of sequence types.

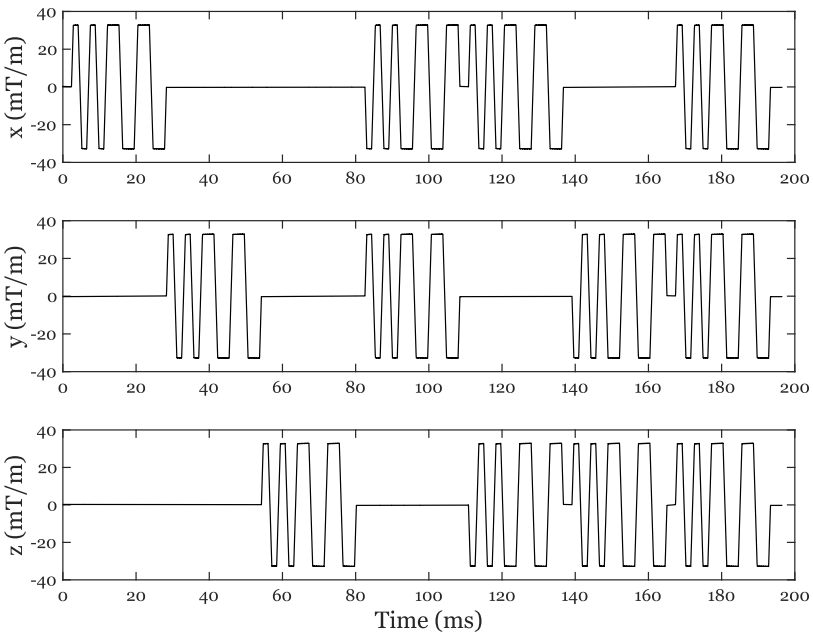

Figure 6. Sequence diagram of test sequence with bipolar gradients, designed for gradient field modeling.

Magnetic field models and exposure metric proxies

In Paper III we presented three different exposure assessment methods (EAM), based on magnetic field measurements, modeling, and identifying proxies for exposure metrics. Direct measurements of the SGF and RF fields (EAM 1) produced a set of exposure metrics describing the exposure at a certain location inside the scanner.

The same set of exposure metrics was produced from approximations of the magnetic fields inside the scanner with analytical models of the output from the SGF and RF coil systems (EAM 2). The gradient B-field model was defined as a function of the sequence diagram waveforms for each gradient coil and the location (coordinates x, y, z) in relation to the scanner isocenter. Based on the assumption of a spatially slow-varying magnetic field, with linear gradients within the imaging field-of-view, we chose a 3rd degree polynomial with spherical harmonics basis functions to represent the gradient B-field. The model was fitted to measured exposure data from multiple locations inside the scanner bore, which allowed us to then approximate B(t) anywhere inside the scanner for any MRI sequence, given access to the gradient waveforms from the specific sequence diagram.

The B_1 field model was defined as a function of the sequence diagram RF pulse waveform, the sequence flip angle, and the RF transmit coil gain. Based on assumptions of spatial homogeneity and the circular polarization of B_1, the relationship between sequence-diagram pulse waveform and $B_1(t)$ shape and amplitude in the transverse plane was assumed to be linear, weighted by parameters flip angle and gain. The model was fitted to measured exposure data including RF pulses of varying types and peak amplitudes, allowing us to then approximate $B_1(t)$ for any MRI sequence given access to the RF pulse waveform from the specific sequence diagram.

As proxies for the metrics produced by the first two methods, we evaluated various parameters related to the SGF and RF fields (EAM 3): estimated dB/dt limit (parameter found in the image metadata), B_{1RMS} (parameter displayed during scanning), whole-body SAR (displayed during scanning), flip angle (from image metadata, sometimes displayed during scanning), and RF transmit coil gain (from image metadata).

Results

While B_0 is constant and homogenous inside the scanner, and therefore easily characterized in terms of exposure, typical SGF and RF fields during an MRI scan are not so easily described. Waveforms and pulse shapes of the time-varying and pulsed magnetic fields can vary significantly between MRI sequences, as shown in Papers I and II. Figure 7 shows examples of measured magnetic field signals with differing gradient waveforms and pulse characteristics.

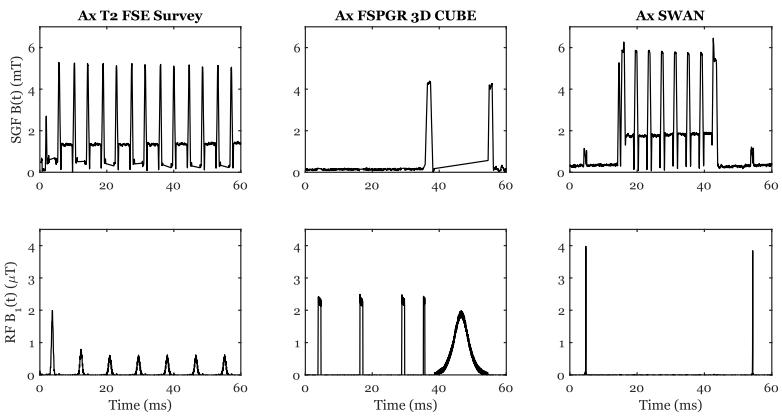

Figure 7. Examples of measured SGF (top panels) and RF (bottom panels) magnetic field signals.

Exposure variability is multi-layered in the MRI exposure environment. Two MRI exams can include different sets of MRI sequences, and two sequences can differ significantly in terms of exposure. The exposure from a single sequence varies with scanner parameter settings, and once the scanning starts, the size and composition of the scanned subject are included in RF power output decisions through the prescan-process. Furthermore, spatial magnetic-field variations introduce a location-based exposure variability that may be of significance in certain circumstances. All these variables make accurate exposure assessment quite challenging.

Exposure variability among MRI sequences

In Paper II we showed that MRI sequences differ from each other in terms of SGF and RF exposure. There was a statistically significant ($p<0.05$) difference in exposure level between two or more sequences for every exposure metric evaluated. Figures 8 and 9 show comparisons between sequences for some exposure metrics.

For some metrics the range between the highest (Exp_{high}) and lowest (Exp_{low}) ranking sequences was small. For example, dB/dt_{max}, the exposure metric describing the maximum gradient field slope during a sequence, was only 50% higher in the Exp_{high} sequence than in the Exp_{low} sequence.

For other metrics the difference was very large relative to the Exp_{low} sequence exposure level. The RF duty cycle, expressed as the percentage of total sequence scan time in which the RF field was being applied, was a metric with a wide range. The Exp_{high} sequence had a duty cycle of 23 % which was 30 times larger than the Exp_{low} sequence with a duty cycle of 0.7 %. Taking the scan time of the two sequences into account revealed a 107-fold difference in total RF field exposure time.

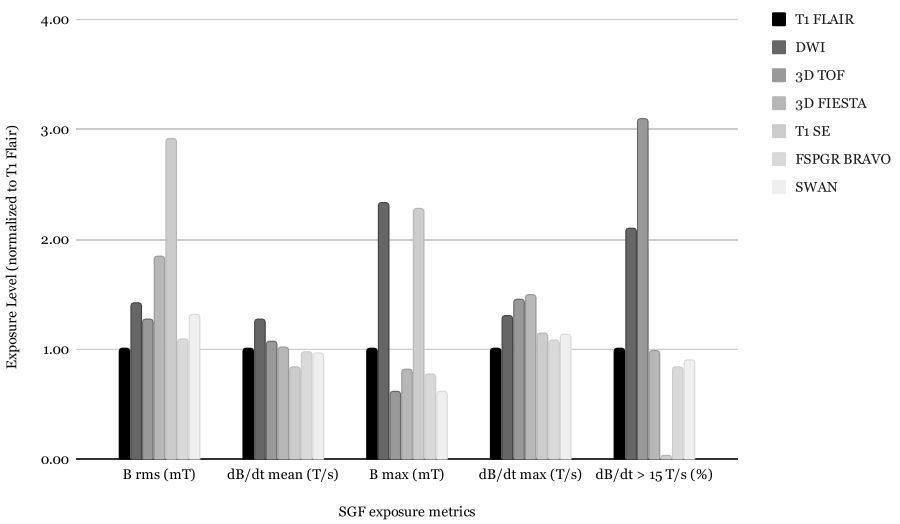

Figure 8. Exposure comparisons between sequences for SGF exposure metrics. All exposure values are normalized to sequence T1 FLAIR to show the variability among the sequences. Mean and peak dB/dt metrics displayed minimal variability while the dB/dt threshold metric showed large differences between sequences of maximum (3D TOF) and minimum (T1 SE) exposure.

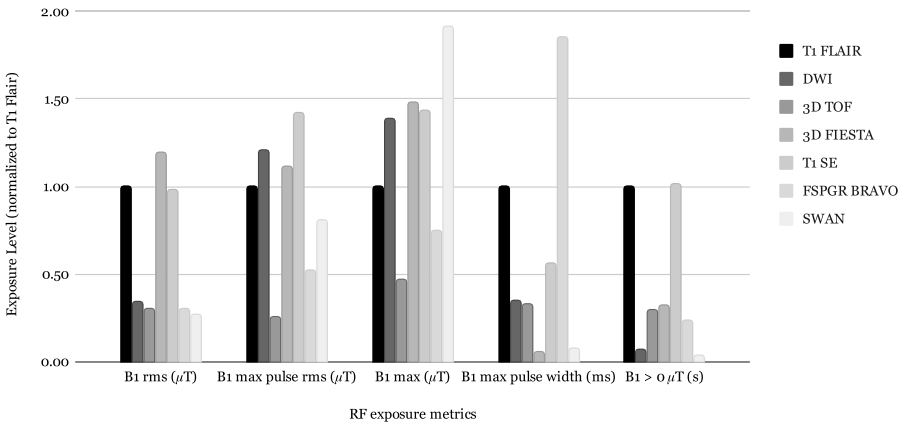

Figure 9. Exposure comparisons between sequences for RF field exposure metrics. All exposure values are normalized to sequence T1 FLAIR to show the variability among the sequences. All metrics display variability.

Exposure variability within an MRI sequence

In addition to the differences in exposure between sequences, a single sequence can generate a range of exposure results depending on the scanner settings. Within-sequence variability investigations on a T_1-weighted FLAIR (fluid-attenuated inversion recovery) sequence, as detailed in Paper II, showed that adjustments to parameters such as flip angle, slice spacing, and field-of-view could produce a 5-to-8-fold increase in exposure. Within-sequence exposure variability was, for some metrics, as much as 60% of the corresponding between-sequence exposure variability found in the same study.

Exposure assessment methods

RF and gradient magnetic fields can be measured inside an MRI scanner, which allows for characterization of the actual exposure experienced at a specific location. Creating models of the scanner's SGF and RF magnetic fields to approximate the exposure at any location is also possible, but we found that certain aspects of the exposure were difficult to predict. Figure 10 shows a few examples of measured and approximated signals for comparison. Our gradient field model generated fairly accurate approximations of B(t) in terms of signal shape, but consistently underestimated the SGF exposure across exposure metrics when compared with the measured signal. The mean difference between the approximated and the measured exposure ranged from -12% to -48% for the SGF model. The RF field model was less consistent, with differences ranging from -5% to +88%, and it resulted in larger differences between approximated and measured RF exposure for certain metrics (Figure 11). Model accuracy can

certainly be improved for both coil systems with further method development. However, the scanner's internal decision processes for SGF and RF field implementation are different, so awareness of those differences is important and will shape the different paths to improved exposure predictability.

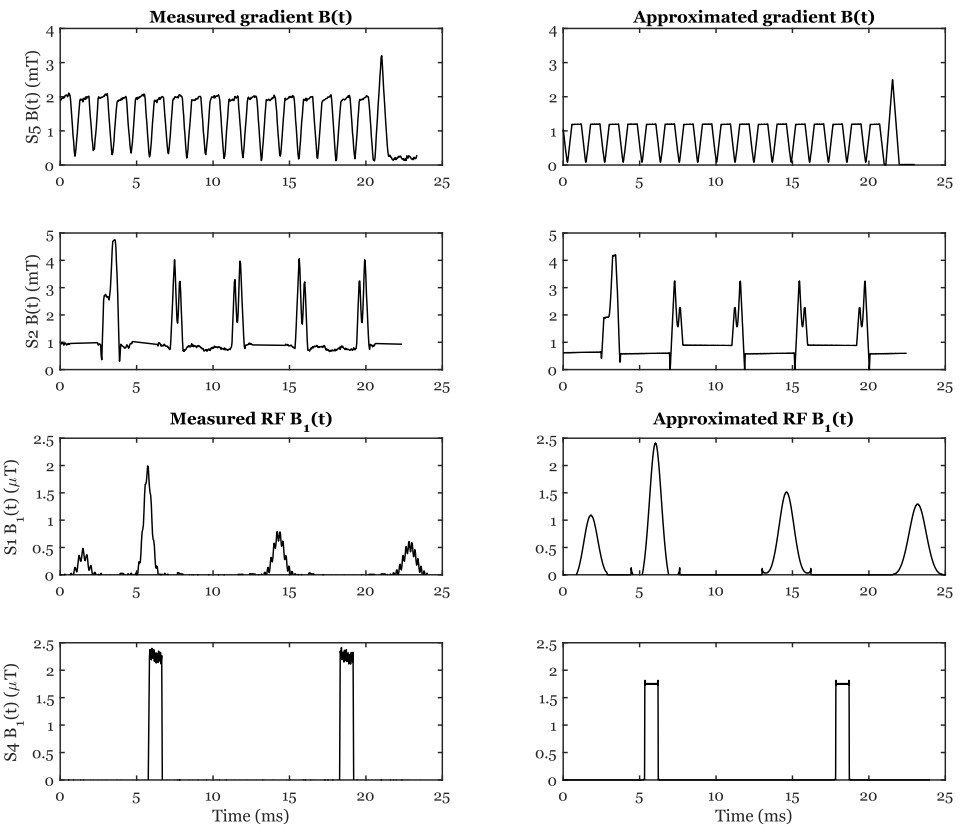

Figure 10. Measured and approximated SGF and RF signals for comparison. The four panels on the left show examples of measured magnetic fields and the panels on the right show their approximated equivalents. Approximated SGF amplitudes (upper two rows) are somewhat smaller than measured amplitudes. Approximated RF amplitudes (lower two rows) are sometimes larger (third row) and sometimes smaller (fourth row) than measured amplitudes. Measurements were taken at (x, y, z) = (10, 13, 14) cm from the scanner isocenter, and the segments shown are from four different sequences, S 5: Ax DWI, S 2: Ax T2 FSE, S 1: Sag T2 FSE Survey, S 4: Sag CUBE FLAIR.

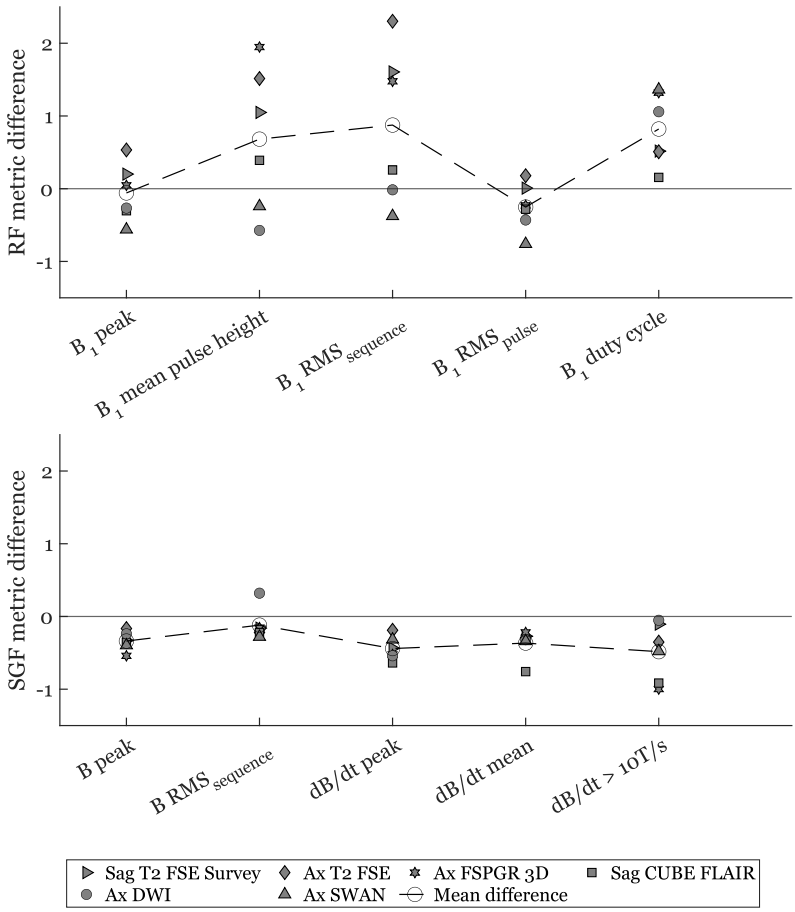

Figure 11. Comparison between modeled and measured exposure metrics for the RF field (upper panel) and the SGF (lower panel). The solid horizontal line in each panel at y = 0 represents the case of no difference between modeled and measured values. The dotted line shows the mean difference between the two methods of exposure assessment. The legend at the bottom of the figure gives the names of the six MRI sequences included in the analysis.

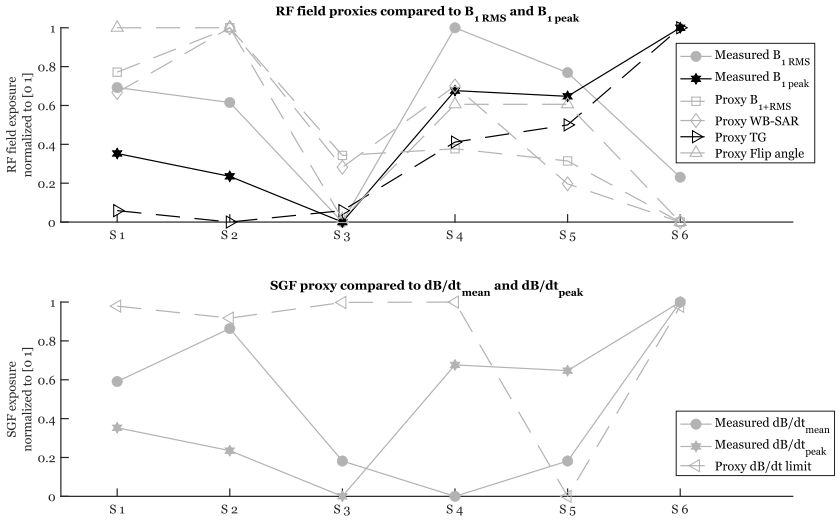

Figure 12. Comparisons between proxies (open markers and dashed lines) and measured exposure metrics (filled markers and solid lines) to see if linear correlation exists. RF field exposure values are shown in the upper panel and SGF exposure values in the lower panel. All values are normalized to the range [0 1]. The sequences included are S 1: Sag T2 FSE Survey, S 2: Ax T2 FSE, S 3: Ax FSPGR 3D PURE, S 4: Sag CUBE FLAIR, S 5: Ax DWI, S 6: Ax SWAN. The one statistically significant ($p < 0.05$) association found was that between the proxy RF coil transmit gain (TG) and the measured B_{1peak} (linear correlation coefficient = 0.92), and these data are shown in black while the others are gray.

In the third exposure assessment method presented in Paper III, our search for suitable SGF and RF exposure proxies resulted in a limited selection (Figure 12), and only one of the proxies (RF coil transmit gain) showed a statistically significant correlation with a measured exposure metric counterpart (B_{1peak}). Further exploration of possible additional proxy candidates, and perhaps combinations of proxies, will be necessary before this method can be truly useful in future research studies.

Spatial field distributions

During our development of a gradient field model for predicting SGF exposure in Paper III we found that the coil system produced concomitant fields, i.e., transverse gradient field components B_x and B_y, on the same order of magnitude as the B_z components (Figure 13).

Orthogonal RF field measurements showed an elliptically rather than circularly polarized B_1 field, with a difference in amplitude between the x-component and the y-component of a factor 2 (Figure 14).

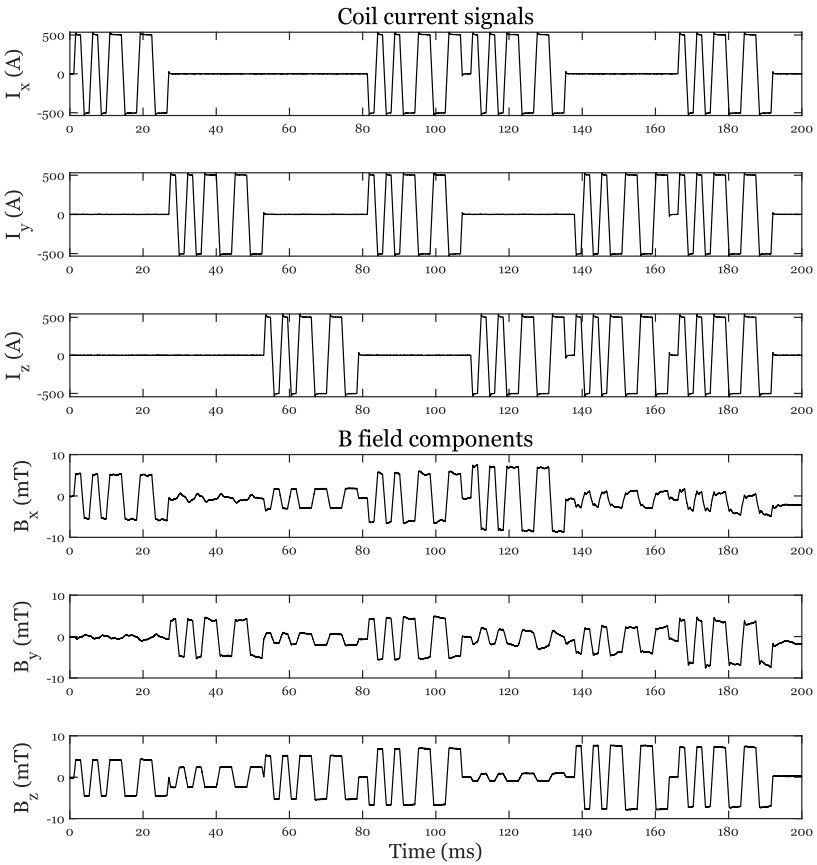

Figure 13. Gradient coil current measurements (upper three panels) and simultaneous measurements of gradient magnetic field components (panels 4-6) taken at (x, y, z) = (17, 13, 15) cm from the scanner isocenter. Each coil contributes to all three B-field components, resulting in measurable transverse components in addition to the image-producing B_z component, sometimes on the same order of magnitude.

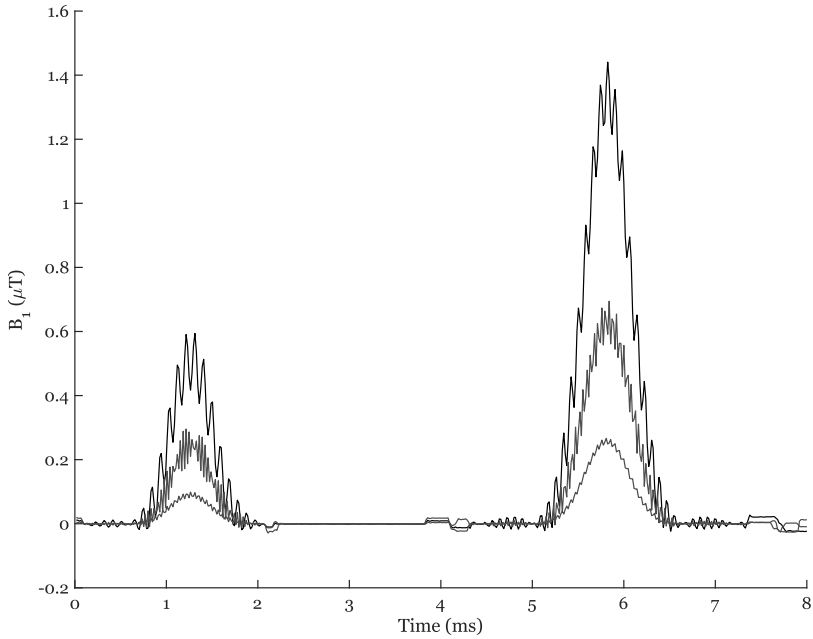

Figure 14. Orthogonal B_1-field components, superimposed to show the differences in amplitude. All three components were measured at (x, y, z) = (10, 4, 10) cm from the scanner isocenter, with the induction coil facing each of the Cartesian axes of the MRI scanner. The amplitude of the x-component is twice that of the y-component, and the z-component is the smallest - barely above noise level.

Discussion

The MRI exposure environment turned out to be somewhat more complex than I had anticipated when I embarked on this research project. The idea of a few basic metrics to describe the exposure experienced in an MRI scanner was very attractive, and a simple method for exposure-classifying exams would be extremely useful in many areas of research. The reality is, however, that the complexity of the time-varying and pulsed magnetic fields makes this unique exposure environment quite difficult to assess.

In comparison with many other exposure agents one might be subjected to, EMFs constitute a complicated form of exposure [8], and the MRI scanner houses a particularly complex mix of non-uniform magnetic fields with varying waveforms and pulses. Magnetic fields with pure sinusoidal waveforms can perhaps be satisfactorily summarized with a couple of parameters such as frequency and peak or RMS amplitude [75], but this is, as shown in Papers I and II, not the case in MRI.

The static magnetic field, B_0, is easily described with a single parameter - the magnetic flux density, since it is rather homogenous within the scanner, but the time-varying fields are more difficult to characterize. The SGF varies temporally and spatially, and the shape and timing of the gradient waveforms varies with sequence design [12]. RF pulses come in varying shapes and amplitudes, and the B_1 duty cycle can differ significantly between sequences, as shown in Paper II. While single-parameter metrics have often been used in past research to describe SGF and RF exposure, such as SAR, dB/dt_{max}, and slew rate [59], they do not capture the full complexity of the exposure. Two MRI sequences could produce identical B_{1RMS} values while consisting of pulse patterns with very different amplitudes and timing. Similarly, the peak dB/dt value could be identical for two sequences, while duration and frequency of occurrence of that peak value differ considerably. I would argue that this level of complexity requires more detailed descriptions of exposure conditions than what we have seen in past research. The ability to clearly describe MRI exposure is increased by having access to a wide range of metrics specifically describing different aspects of the magnetic fields – such as the ones presented in this thesis.

The multi-level exposure variability shown in Paper II makes exposure classification of clinical MRI exams especially complicated. An MRI exam of a brain may or may not differ from a knee exam in terms of exposure, so an exposure description that only gives the exam type, e.g., “a standard cardiac protocol”, is woefully unspecific. It all depends upon which sequences are included in the exam protocol. Two sequences can differ significantly in exposure,

and they need to be individually evaluated before a complete exam can be meaningfully assessed and classified in terms of exposure.

Furthermore, the potential for within-sequence exposure variability, due to changeable parameter settings at the scanner console, means that an MRI sequence cannot easily be classified by name alone. The same sequence can generate quite different exposure levels depending on the choice of e.g., flip angle or field-of-view. Hence, the exposure needs to be described in terms of the characteristics of the magnetic fields, and awareness of the many factors that affect the ultimate exposure output of an MRI sequence is important. This includes the parameter settings that are changeable by the scanner technician at the console.

In past *in vivo* studies, exposure descriptions have sometimes been minimal, such as "a standard cardiac examination" [49], or with a little more detail such as the use of "cardiac MRI" and brief mentions of sequences used plus a clarification that scanning duration was "roughly between 40 and 50 min" for the scanned volunteers [58]. With such limited information we do not know much about the exposure, except that in the latter case there were, perplexingly, differences in scanning duration among the participants. Results from such studies are difficult to evaluate, and awareness of the inherent exposure variability in MRI exams and individual sequences is important for future experimental research involving MRI. Exposure assessment must be specific enough to take this variability into account so that exposure conditions can be replicated, and study results can be properly evaluated and compared.

Clinical exams generally include multiple sequences, which can vary significantly in exposure. How to best combine the metrics from several sequences into one total exposure value for the entire exam depends entirely on the choice of exposure metric. The choice of exposure metric(s), in turn, should be guided by the research study hypothesis, as we recently discussed [59]. If mean values such as B_{1RMS}, or threshold values such as $dB/dt_{\%>10T/s}$, are assumed to be of most importance biologically, perhaps the values from each sequence, weighted by the sequence scan time, could be summed up into a combined exposure value for the entire exam, similar to the way Simi et al. [49] used time-weighted SAR values to express RF exposure. If, on the other hand, peak values such as B_{1peak} or dB/dt_{peak} are considered biologically relevant, the maximum value among the sequences could be chosen to represent the entire exam. In many cases the SGF exposure of an entire exam protocol has been summarized by simply stating the maximum field strength (measured in mT/m) and slew rate (measured in T/m/s) of the gradient coil system [52, 53, 69]. However, this kind of generalization does not take exposure variability between sequences into account, it is a very blunt

measure of SGF exposure, and it is impossible to judge whether the maximum levels had even been reached during scanning.

In Papers II and III we presented several different exposure metrics specifically describing various aspects of the magnetic fields in the MRI exposure environment, rather than internal electric fields in scanned subjects. We know that external magnetic fields induce internal electric fields in the human body [3], so it makes sense to focus on them during exposure assessment. After all, the interactions between the magnetic fields and biological tissue, and any resulting effects, happen internally. Internal electric fields, however, are notoriously difficult to measure, so they generally have to be estimated through numerical simulation which can be quite complex and computationally expensive [64], and such patient-dependent dosimetry is not realistic for large-scale epidemiological studies [63]. With our methods and metrics, specifically focused on magnetic field characteristics, we hope to provide useful tools for epidemiological research on MRI patients and long-term health effects. *In vitro* studies, with clearly defined exposure conditions, and identical size-, composition-, and placement parameters for all exposed samples, provide a more controlled study environment where internal field simulations may be quite relevant [76]. However, with a clinical MRI scanner as the source of exposure, a lot of variability is introduced. With a mix of gradient waveforms and RF pulses with varying amplitudes and temporal spacing, it may be desirable to define exposure in terms of the characteristics of the external magnetic field. Thereby exposure classification could be based on a specific exposure feature hypothesized to impact the tissue, e.g., peak or RMS amplitude, duty cycle, timing of waveforms, peak dB/dt, rise time for a certain threshold dB/dt value. In our continued search for answers about the interaction mechanisms we need to be very specific about the exposure applied.

To answer questions about MRI and long-term health effects both epidemiological and experimental research are needed [7]. Both types of research require exposure assessment methods that clearly define the exposure involved and allow for some form of classification. It is difficult to draw any conclusions about whether MRI exams can cause DNA damage based on the existing body of research on MRI and genotoxicity because of the mixed results [77] and the lack of information about the exposure conditions involved [59]. We have suggested a range of SGF and RF exposure metrics that describe various features of the magnetic field exposure, such as mean, peak and threshold values, and there are surely others of interest as well. Future research will need to uncover which aspects of MRI exposure matter biologically. Hopefully, together with clear hypotheses about the interaction mechanisms involved, our approach to exposure assessment will lead to improved research quality in future studies.

The reasoning behind our measurement-based assessment methods was that measuring B(t) and $B_1(t)$ inside the scanner gives a true picture of the magnetic field exposure present during a scan, with a relatively modest set of assessment equipment. Detailed analytical calculations of the magnetic fields produced inside an MRI scanner are an important part of the scanner design- and manufacturing process [16], but would require intimate knowledge of coil designs and surrounding materials – information which is not readily available to the average exposure researcher. Numerical simulations of induced electric fields are highly dependent on the specific features of the human models used and can be computationally expensive as well as difficult to verify [64]. Our proposed method of measuring magnetic fields and analyzing the B(t) and $B_1(t)$ signals to determine exposure sidesteps such issues, and allows for precise exposure assessment at a specific location. This is especially suitable for *in vitro* studies on MRI and cellular-level effects, if there is a limited and pre-defined exposure protocol and a specified exposure location. Previous studies, with their methodological issues and inadequate exposure characterizations [77, 78], can perhaps be considered hypothesis-generating, and now we need to move on to hypothesis-testing studies, with precise exposure assessments and easily compared exposure metrics.

Approximating SGF and RF exposure based on models fitted to experimental data, as described in exposure assessment method 2 from Paper III, could make a wider range of exposure assessments available. Once the initial model-building is done, the exposure of any sequence can be estimated at any location. This could be useful for *in vitro* and *in vivo* studies with large or varied exposure protocols. Characterizing a whole scanner system in terms of exposure, rather than a single MRI sequence, could also prove useful in clinical work. Safety-evaluations of medical implants could be based on more detailed exposure assessments than the SAR and dB/dt limit values presented by scanners today [4]. While there is room for improvement, our first iteration of the method shows promise, and with further development the method could prove useful in a variety of situations on a range of MRI systems.

While our SGF model was quite consistent, the RF field model showed less agreement with measured data. There are several reasons for this, and the main issue was the limited input information. The general shape of an RF pulse is already decided in the sequence design [12], but features such as amplitude and timing between pulses can be affected by choices made by the technician at the console, e.g., flip angle, echo time and repetition time settings. Furthermore, additional factors are determined during the automated calibration process of the sequence prescan [11], and can possibly only be learned after the fact. This means that an approximation based only on sequence design pulse waveforms is very limited, and modeling accuracy depends on which additional RF pulse decision

factors one has access to. Our model included flip angle and RF coil transmit gain values, but some sequences include multiple RF pulses with different flip angles – not necessarily adjustable at the console, so much of the decision process leading up to the final output from the RF coil was unavailable to us. Also, our assumptions of a spatially homogenous and circularly polarized B_1 field may have been too simplistic. Interactions between the RF field and biological tissue, causing image inhomogeneity and tissue heating, have driven RF transmit coil design development towards more complex configurations, which use B_1 shimming to mitigate internal inhomogeneity [16]. One effect which can result from these advancements is a more elliptically polarized RF field when measured without a patient present, which matches our results of a difference in amplitude between the x- and y-components of the B_1 field.

There is room for improvement in both of our models, especially in the RF field approximation. Our goal here was to present a prototype for an exposure assessment method based on EMF modeling, and we have shown that the SGF and RF fields can be approximated with some degree of accuracy. With various modifications to the models, and certain scanner-specific adjustments depending on one's MRI system, this exposure assessment method could hopefully become a useful tool in future research and clinical work.

As model-input we chose to use waveform diagrams because of the relative ease of acquiring them on our MRI system, and because they provided a significant amount of information about the magnetic fields of a sequence. However, there were some limitations to this approach, including the lack of information about amplitude variations over time due to, e.g., gradually increasing phase-encoding gradients and variable flip angles. Such issues could be solved by using a more dynamic model input such as the coil current control signals – as Trevisan et al. [65] did in their slew rate evaluation approach, and in a future implementation of this method we intend to try that.

The third method described in Paper III, which involved identifying suitable proxies for measured exposure metrics, would be ideal for large-scale exposure assessment such as in epidemiological research. The ability to classify a scan based on image metadata would allow for retroactive exposure analysis of image databases, increasing our possibilities to find connections between MRI and possible long-term health effects. The most readily available exposure information of, e.g., scanner-estimated SAR and maximum gradient coil strength and speed, is not very practical for exposure classification of sequences. Such metrics are blunt and unreliable, because, as we saw in Paper II, exposure differences between sequences range from small to very large, depending on the specific SGF or RF metric under comparison. A strong correlation between a chosen proxy and its exposure metric counterpart is required, and further

investigation is needed to find good proxies for the metrics described in this thesis. It would be of interest to include multiple MRI systems in future method development as different exposure-related information may be available from different scanners [1].

During exposure assessment method development, we looked at individual gradient field components, B_x, B_y, and B_z, and their relationships to the electrical currents running through the three gradient coils. We found that, at certain measurement locations and for various combinations of applied gradients, transverse components could be of the same magnitude as B_z. While this may seem unintuitive, or at least somewhat impractical, as B_z is the only wanted gradient field component for image creation, it is completely in line with the electromagnetic principles described by Maxwell's equations [15]. These concomitant fields have been described in MRI literature since 1990 [17], and the challenge has been to correct for them in image-construction to avoid gradient non-linearity distortions [18]. As main field strengths have increased, the total impact of the concomitant fields on image quality has decreased, but even though the concomitant fields can be small or even negligible from an image-distortion point-of-view, they are always present when gradients are applied and therefore part of the total gradient magnetic field exposure experienced by the scanned subject [12].

In Papers II and III we chose to study MRI protocols typically used in regular clinical exams, as that is the form in which patients and research subjects are generally exposed to MRI-related magnetic fields. Meaningful exposure classification requires an understanding of the structure and multi-level exposure variability of clinical MRI exams. Because MRI has become so ubiquitous, a considerable portion of the human population will get a scan sometime during their lifetime, and a portion of that group may experience frequent MRI exams. This is relevant because, while the acute exposure effects of MRI are well known and regulated, possible long-term health effects are not considered in safety guidelines and exposure limits [4, 5, 31, 32]. I would argue that both acute and chronic effects should be included in a risk-benefit analysis whenever an exposure environment such as the MRI scanner is employed, but unfortunately an informed risk-benefit analysis is not possible at this time, since risks of long-term health effects – however small they may be – are not yet fully understood.

The sequences evaluated in Paper II were from a standard pediatric brain scan protocol. A pediatric exam protocol is not inherently different from one used for adults. In fact, they can include the same sequences. Instead, scanner mode and various scanner parameter settings may be adjusted to adapt sequences for use in vulnerable populations [79, 80]. Of all the patient groups who would benefit from us having a more comprehensive understanding of the MRI exposure

environment, perhaps the youngest stand to gain the most. In addition to children being especially sensitive to electromagnetic field exposure because of their still-developing nervous systems [81], they also have their whole lives ahead of them in which to develop possible long-term health effects and to experience additional exposure. So, as the application of MRI grows worldwide, both for adults and children, it becomes increasingly important that we strive to reach a comprehensive understanding of this unique exposure environment.

During the work in this thesis, I have had the privilege of being able to approach the MRI exposure environment with a large dose of curiosity, frequent access to an MRI scanner, and a practical set of measurement equipment. Many long scanner-sessions were spent adjusting probe positions and scanner settings and ruminating on unexpected waveforms. This journey into the world of imaging physics, magnetic field exposure, and signal processing has been fascinating and educational. Measuring the actual magnetic fields during an MRI scan, and then plotting the signals as functions of time, has been very helpful in understanding what goes on inside the MRI scanner. The MRI scanner presents a complex exposure environment, and accurately measuring time-varying and pulsed magnetic fields inside a strong static field can be difficult. When assessing SGF and RF fields, with differing frequency, intensity, and spatial distribution, cross-contamination between signals can be an issue. In our case the gradient field impact on the RF signal was minor while distortions of the SGF signal caused by the RF field required significant post-processing to avoid undue impact on the results. Another challenge with these types of measurements is to determine the total magnetic field at a certain point, including all three orthogonal components. With our commercial B-field probe we could capture the gradient field components simultaneously and thereby get a real-time measurement of the combined $B_{tot}(t)$ signal. From an exposure perspective this is important since the scanned subject experiences all components of the magnetic field simultaneously, regardless of whether the components are part of the image-specific spatial encoding or not. For RF field analysis we had a one-dimensional measuring probe, which we deemed sufficient for the task because of the symmetry of the B_1 field [11]. However, it would have been interesting to see simultaneous measurements of orthogonal B_1 components, and perhaps that will be possible in future work.

A limitation of this thesis is the scope of the empirical work. Measurements were performed on a single scanner system due to practical restrictions, but it would have been interesting to look at exposure variability across multiple systems and test our assessment methods on different scanners. Also, any type of measurement equipment will have some limitations, and working in a unique exposure environment such as the MRI scanner poses several challenges to the processes of data acquisition and analysis. Our probes were designed and

calibrated for the specific frequency ranges they were employed to measure, but both measured magnetic field signals had interference from each other. SGF noise in the measured RF data was minimal, but RF influence on the SGF signal B(t) was clearly visible, requiring significant post-processing.

This thesis does not reveal which, if any, features of MRI exposure cause long-term health effects, or what those effects might be. Such questions have proven very difficult to answer in the past, in part because EMF exposure assessment is quite complicated [8, 75], and also because the effects under investigation have been so elusive. Despite the vast amount of EMF exposure research performed to date, the results are still inconclusive and often conflicting [46, 62]. This is probably due both to methodological issues and to the complexity of the interactions between low-frequency magnetic fields and biological tissue, including, e.g., coherence dependencies and various biological feedback processes [6, 48]. The work in this thesis has been aimed at increasing our awareness of MRI-related magnetic fields and providing exposure assessment tools relevant to the unique MRI exposure environment. Hopefully, these tools can, together with an increased understanding of SGF and RF field characteristics and exposure variability, provide a valuable contribution in the quest for answers about MRI and long-term health effects.

With the measurement-based method (EAM 1) presented in Paper III, a detailed description of the SGF and RF field exposure can be acquired for any MRI exam protocol, as long as the location inside the scanner is specified. This is relevant for anyone planning an *in vitro* study in the MRI environment, and I hope this approach will be employed in future research on MRI and genotoxicity. I believe the method can improve research quality by increasing study reproducibility with more comprehensive exposure descriptions than we have previously seen.

The calculation-based method (EAM 2) requires further development before it can be put to use clinically or in research. Some improvement strategies were suggested for increased accuracy, such as more comprehensive spatial test measurements and the use of coil current control signals rather than a waveform diagram as model input. I believe this approach to exposure assessment is very promising, and, once an acceptable level of model accuracy has been reached, the method will prove useful in a wide range of *in vitro* and *in vivo* research settings. Evaluation of standard protocols could also be useful in day-to-day clinical work, identifying high-exposure sequences and high-intensity locations inside the scanner. Such applications of the method could be an asset in implant safety assessments by providing more specific exposure assessments for the MRI sequences of interest.

The proxy method (EAM 3) needs additional development before it can be useful in research-related exposure classification of MRI sequences. Further exploration of possible exposure metric proxies is warranted, ideally on scanner systems from multiple manufacturers, as they may provide different information related to the magnetic fields involved. A viable version of this method would be very useful in large-scale epidemiological investigations of patients or research volunteers who have undergone MRI exams.

Conclusion

In conclusion, the work in this thesis has contributed to our increased understanding of the unique MRI scanner environment from an exposure perspective, by characterizing the exposure in terms of inherent features of the magnetic fields involved. While the main field, B_0, is easily described with a single measure of the static magnetic flux density, the SGF and RF magnetic fields create a complex mix of waveforms and pulses with varying amplitudes, frequencies, and timing. Spatial as well as temporal variability makes the SGF and RF exposure much more difficult to define.

Significant exposure variability exists between MRI sequences, sometimes with more than a 100-fold difference between sequences for certain exposure metrics. This means that exams consisting of multiple sequences are not homogenous in terms of exposure, and they need to be classified on the individual sequence-level. Furthermore, a several-fold increase in exposure from a single MRI sequence can result from parameter adjustments at the scanner console, so awareness of within-sequence exposure variability due to impact from scanner parameter settings and patient characteristics is also important for meaningful exposure classification of clinical MRI exams.

With exposure metrics describing explicit features of the magnetic fields rather than estimations of induced internal electric fields, the exposure environment can be more easily studied, and MRI exposure classification becomes available for large-scale investigations. Our suggested metrics describe the SGF and RF field exposure in terms of mean, peak, and threshold values, providing a detailed characterization of the exposure environment.

Measurement-based exposure assessment methods and metrics, such as those presented in this thesis, are specifically suited to the complex MRI exposure environment, and provide the tools for performing meaningful exposure assessments in future studies on MRI and long-term health effects, in much needed experimental and epidemiological research.

Acknowledgements

I am truly grateful for my amazing network of family, friends, and coworkers, who have helped and cheered me on during my years as a PhD student. In my supervisors I have found excellent teachers and role models, and I have felt supported and encouraged every step of the way. I am also lucky to have such a delightful group of colleagues, always up for serious scientific discussions as well as friendly fun and games. Last, but certainly not least, I am incredibly thankful for all the help and support from my wonderful family and friends – thank you for being you, and for believing in me.

References

1. McRobbie, D.W., *Essentials of MRI safety*. First ed. 2020, Hoboken, NJ: Wiley-Blackwell.

2. Elster, A.D. and J.H. Burdette, *Questions & Answwers in Magnetic Resonance Imaging*. Second ed. 2001, St. Louis, MO: Mosby, Inc.

3. Reilly, J.P., *Applied Bioelectricity. From Electrical Stimulation to Electropathology*. 1998, New York, NY: Springer-Verlag.

4. CENELEC, *Medical electrical equipment - Part 2-33: Particular requirements for the basic safety and essential performance of magnetic resonance equipment for medical diagnosis.*, in *CENELEC EN 60601-2-33:2010/A12:2016*. 2016: Brussels, Belgium.

5. European Parliament and Council of the European Union, *Directive 2013/35/EU of the European Parliament and of the Council of 26 June 2013 on the minimum health and safety requirements regarding the exposure of workers to the risks arising from physical agents (electromagnetic fields) (20th individual Directive within the meaning of Article 16(1) of Directive 89/391/EEC) and repealing Directive 2004/40/EC*, European Parliament - Legislative observatory, Editor. 2013, The Member States,: OJ L 179, 29.6.2013, p. 1–21.

6. Barnes, F. and B. Greenebaum, *Setting guidelines for electromagnetic exposures and research needs*. Bioelectromagnetics, 2020. **41**(5): p. 392-397.

7. SCENIHR, *Potential health effects of exposure to electromagnetic fields (EMF)*. 2015, Scientific Committee on Emerging and Newly Identified Health Risks, European Commission: Luxembourg. Accessed at https://ec.europa.eu/health/sites/health/files/scientific_committees/emerging/docs/scenihr_o_041.pdf on 2021-04-13.

8. Valberg, P.A., *Designing EMF experiments: what is required to characterize "exposure"?* Bioelectromagnetics, 1995. **16**(6): p. 396-401 discussion 402-406.

9. Hansson Mild, K. and M.O. Mattsson, *Dose and Exposure in Bioelectromagnetics*, in *Dosimetry in Bioelectromagnetics*, M. Markov, Editor. 2017, CRC Press: Boca Raton, FL. p. 101-117.

10. Lauterbur, P., *Image formation by induced local interactions: examples employing nuclear magnetic resonance*. Nature, 1973. **242**: p. 190-191.

11. McRobbie, D.W., et al., *MRI From Picture to Proton*. Second ed. 2007, New York, NY: Cambridge University Press.

12. Bernstein, M.A., K.F. King, and X.J. Zhou, *Handbook of MRI Pulse Sequences*. First ed. 2004, Burlington, MA: Elsevier Academic Press.

13. Levitt, M.H., *Spin Dynamics. Basics of Nuclear Magnetic Resonance*. Second ed. 2015, Chichester, UK: Wiley.

14. Demarest, K.R., *Engineering Electromagnetics*. 1998, Upper Saddle River, NJ: Prentice-Hall.

15. Hidalgo-Tobon, S.S., *Theory of gradient coil design methods for magnetic resonance imaging*. Concepts in Magnetic Resonance, 2010. **36A**(4): p. 223-242.

16. Chen, X. and M. Steckner, *Electromagnetic computation and modeling in MRI*. Med Phys, 2017. **44**(3): p. 1186-1203.

17. Norris, D.G. and J.M. Hutchison, *Concomitant magnetic field gradients and their effects on imaging at low magnetic field strengths*. Magn Reson Imaging, 1990. **8**(1): p. 33-37.

18. Bernstein, M.A., et al., *Concomitant gradient terms in phase contrast MR: analysis and correction*. Magn Reson Med, 1998. **39**(2): p. 300-308.

19. Gruber, B., et al., *RF coils: A practical guide for nonphysicists*. J Magn Reson Imaging, 2018. **48**(3): p. 590-604.

20. McJury, M. and F.G. Shellock, *Auditory noise associated with MR procedures: a review*. J Magn Reson Imaging, 2000. **12**(1): p. 37-45.

21. Wilén, J. and F. de Vocht, *Health complaints among nurses working near MRI scanners--a descriptive pilot study*. Eur J Radiol, 2011. **80**(2): p. 510-513.

22. Batistatou, E., et al., *Personal exposure to static and time-varying magnetic fields during MRI procedures in clinical practice in the UK*. Occup Environ Med, 2016. **73**(11): p. 779-786.

23. de Vocht, F., et al., *Transient health symptoms of MRI staff working with 1.5 and 3.0 Tesla scanners in the UK*. Eur Radiol, 2015. **25**(9): p. 2718-2726.

24. Andreuccetti, D., et al., *Occupational exposure in MR facilities due to movements in the static magnetic field*. Med Phys, 2017. **44**(11): p. 5988-5996.

25. Schaap, K., L. Portengen, and H. Kromhout, *Exposure to MRI-related magnetic fields and vertigo in MRI workers*. Occup Environ Med, 2016. **73**(3): p. 161-166.

26. Zanotti, G., G. Ligabue, and F. Gobba, *Subjective symptoms and their evolution in a small group of magnetic resonance imaging (MRI) operators recently engaged*. Electromagn Biol Med, 2015. **34**(3): p. 262-264.

27. Hansson, B., et al., *Short-term effects experienced during examinations in an actively shielded 7 T MR*. Bioelectromagnetics, 2019. **40**(4): p. 234-249.

28. Reilly, J.P., *Principles of nerve and heart excitation by time-varying magnetic fields*. Ann N Y Acad Sci, 1992. **649**: p. 96-117.

29. Glover, P.M., *Interaction of MRI field gradients with the human body*. Phys Med Biol, 2009. **54**(21): p. R99-R115.

30. El-Sharkawy, A.M., et al., *A multichannel, real-time MRI RF power monitor for independent SAR determination*. Medical Physics, 2012. **39**(5): p. 2334-2341.

31. ICNIRP, *Guidelines for limiting exposure to time-varying electric and magnetic fields (1 Hz to 100 kHz)*. Health Phys, 2010. **99**(6): p. 818-836.

32. ICNIRP, *Guidelines for Limiting Exposure to Electromagnetic Fields (100 kHz to 300 GHz)*. Health Phys, 2020. **118**(5): p. 483-524.

33. Wertheimer, N. and E. Leeper, *Electrical wiring configurations and childhood cancer*. Am J Epidemiol, 1979. **109**(3): p. 273-284.

34. Ahlbom, A., et al., *A pooled analysis of magnetic fields and childhood leukaemia*. Br J Cancer, 2000. **83**(5): p. 692-698.

35. Greenland, S., et al., *A pooled analysis of magnetic fields, wire codes, and childhood leukemia. Childhood leukemia-EMF study group*. Epidemiology, 2000. **11**(6): p. 624-634.

36. Kheifets, L., et al., *Residential magnetic fields exposure and childhood leukemia: a population-based case-control study in California*. Cancer Causes Control, 2017. **28**(10): p. 1117-1123.

37. INTERPHONE, *Brain tumour risk in relation to mobile telephone use: results of the INTERPHONE international case-control study*. Int J Epidemiol, 2010. **39**(3): p. 675-694.

38. Hardell, L., M. Carlberg, and K. Hansson Mild, *Pooled analysis of case-control studies on malignant brain tumours and the use of mobile and cordless phones including living and deceased subjects*. Int J Oncol, 2011. **38**(5): p. 1465-1474.

39. Schüz, J., et al., *Cellular telephone use and cancer risk: update of a nationwide Danish cohort*. J Natl Cancer Inst, 2006. **98**(23): p. 1707-1713.

40. Holland, S.K., et al., *Data on the safety of repeated MRI in healthy children*. Neuroimage Clin, 2014. **4**: p. 526-530.

41. Bongers, S., et al., *Exposure to static magnetic fields and risk of accidents among a cohort of workers from a medical imaging device manufacturing facility*. Magn Reson Med, 2016. **75**(5): p. 2165-2174.

42. Huss, A., K. Schaap, and H. Kromhout, *A survey on abnormal uterine bleeding among radiographers with frequent MRI exposure using intrauterine contraceptive devices*. Magn Reson Med, 2018. **79**(2): p. 1083-1089.

43. Bongers, S., P. Slottje, and H. Kromhout, *Development of hypertension after long-term exposure to static magnetic fields among workers from a magnetic resonance imaging device manufacturing facility*. Environ Res, 2018. **164**: p. 565-573.

44. Huss, A., et al., *Occupational exposure to MRI-related magnetic stray fields and sleep quality among MRI - Technicians - A cross-sectional study in the Netherlands*. Int J Hyg Environ Health, 2021. **231**: p. 113636.

45. Sheppard, A.R., M.L. Swicord, and Q. Balzano, *Quantitative evaluations of mechanisms of radiofrequency interactions with biological molecules and processes*. Health Phys, 2008. **95**(4): p. 365-396.

46. Vijayalaxmi, Y. Cao, and M.R. Scarfi, *Adaptive response in mammalian cells exposed to non-ionizing radiofrequency fields: A review and gaps in knowledge*. Mutat Res Rev Mutat Res, 2014. **760**: p. 36-45.

47. Litovitz, T.A., D. Krause, and J.M. Mullins, *Effect of coherence time of the applied magnetic field on ornithine decarboxylase activity*. Biochem Biophys Res Commun, 1991. **178**(3): p. 862-865.

48. Hansson Mild, K. and M.O. Mattsson, *ELF noise fields: a review*. Electromagn Biol Med, 2010. **29**(3): p. 72-97.

49. Simi, S., et al., *Is the genotoxic effect of magnetic resonance negligible? Low persistence of micronucleus frequency in lymphocytes of*

individuals after cardiac scan. Mutation Research/Fundamental and Molecular Mechanisms of Mutagenesis, 2008. **645**(1-2): p. 39-43.

50. Lee, J.W., et al., *Genotoxic effects of 3 T magnetic resonance imaging in cultured human lymphocytes*. Bioelectromagnetics, 2011. **32**(7): p. 535-542.

51. Fiechter, M., et al., *Impact of cardiac magnetic resonance imaging on human lymphocyte DNA integrity*. European Heart Journal, 2013. **34**(30): p. 2340-2345.

52. Lancellotti, P., et al., *Biological effects of cardiac magnetic resonance on human blood cells*. Circ Cardiovasc Imaging, 2015. **8**(9): p. e003697.

53. Critchley, W.R., et al., *The effect of 1.5 T cardiac magnetic resonance on human circulating leucocytes*. Eur Heart J, 2018. **39**(4): p. 305-312.

54. Szerencsi, Á., et al., *DNA integrity of human leukocytes after magnetic resonance imaging*. International Journal of Radiation Biology, 2013. **89**(10): p. 870-876.

55. Reddig, A., et al., *Analysis of DNA double-strand breaks and cytotoxicity after 7 Tesla magnetic resonance imaging of isolated human lymphocytes*. PLOS ONE, 2015. **10**(7): p. e0132702.

56. Fatahi, M., et al., *DNA double-strand breaks and micronuclei in human blood lymphocytes after repeated whole body exposures to 7T Magnetic Resonance Imaging*. Neuroimage, 2016. **133**: p. 288-293.

57. Brand, M., et al., *Influence of Cardiac MR Imaging on DNA Double-Strand Breaks in Human Blood Lymphocytes*. Radiology, 2015. **277**(2): p. 406-412.

58. Fasshauer, M., et al., *Absence of DNA double-strand breaks in human peripheral blood mononuclear cells after 3 Tesla magnetic resonance imaging assessed by γH2AX flow cytometry*. Eur Radiol, 2018. **28**(3): p. 1149-1156.

59. Wilén, J., et al., *Valid exposure protocols needed in magnetic resonance imaging genotoxic research*. Bioelectromagnetics, 2020. **41**(3): p. 247-257.

60. IARC, *Non-ionizing radiation, Part 1: static and extremely low-frequency (ELF) electric and magnetic fields*. IARC Monogr Eval Carcinog Risks Hum, 2002. **80**: p. 1-395.

61. IARC, *Non-ionizing radiation, Part 2: Radiofrequency electromagnetic fields*. IARC Monogr Eval Carcinog Risks Hum, 2013. **102**(Pt 2): p. 1-460.

62. Vijayalaxmi, M. Fatahi, and O. Speck, *Magnetic resonance imaging (MRI): A review of genetic damage investigations*. Mutat Res Rev Mutat Res, 2015. **764**: p. 51-63.

63. Röösli, M. and D. Vienneau, *Epidemiology of Electromagnetic Fields*. First ed. 2014, Boca Raton, FL: CRC Press.

64. Kabil, J., et al., *A review of numerical simulation and analytical modeling for medical devices safety in MRI*. Yearb Med Inform, 2016. **25**(1): p. 152-158.

65. Trevisan, D., et al., *Magnetic resonance examination of patients with implanted pacemakers: An evaluation of magnetic field gradients slew rate*. Bioelectromagnetics, 2017. **38**(4): p. 307-314.

66. Hartwig, V., *Engineering for safety assurance in MRI: analytical, numerical and experimental dosimetry*. Magnetic Resonance Imaging, 2015. **33**(5): p. 681-689.

67. Murbach, M., et al., *Whole-body and local RF absorption in human models as a function of anatomy and position within 1.5T MR body coil*. Magn Reson Med, 2014. **71**(2): p. 839-845.

68. Zilberti, L., et al., *Numerical prediction of temperature elevation induced around metallic hip prostheses by traditional, split, and uniplanar gradient coils*. Magn Reson Med, 2015. **74**(1): p. 272-279.

69. Yildiz, S., et al., *Impact of contrast enhanced MRI on lymphocyte DNA damage and serum visfatin level*. Clin Biochem, 2011. **44**(12): p. 975-979.

70. Suntharalingam, S., et al., *Abdominopelvic 1.5-T and 3.0-T MR imaging in healthy volunteers: relationship to formation of DNA double-strand breaks*. Radiology, 2018. **288**(2): p. 529-535.

71. Hansson Mild, K., et al., *How to combine the use of different mobile and cordless telephones in epidemiological studies on brain tumours?* Eur J Cancer Prev, 2005. **14**(3): p. 285-288.

72. Wilén, J., M. Sandström, and K. Hansson Mild, *Subjective symptoms among mobile phone users--a consequence of absorption of radiofrequency fields?* Bioelectromagnetics, 2003. **24**(3): p. 152-159.

73. Inyang, I., et al., *Comparison of measuring instruments for radiofrequency radiation from mobile telephones in epidemiological studies: implications for exposure assessment*. J Expo Sci Environ Epidemiol, 2008. **18**(2): p. 134-141.

74. Hansson Mild, K., et al., *Exposure classification of MRI workers in epidemiological studies*. Bioelectromagnetics, 2013. **34**(1): p. 81-84.

75. Kaune, W.T., *Comment on "designing EMF experiments: what is required to characterize 'exposure'?"*. Bioelectromagnetics, 1995. **16**(6): p. 402-404.

76. Schönborn, F., et al., *Basis for optimization of in vitro exposure apparatus for health hazard evaluations of mobile communications*. Bioelectromagnetics, 2001. **22**(8): p. 547-559.

77. Fatahi, M., et al., *MRI and genetic damage: an update*. Current Radiology Reports, 2017. **5**: p. 20.

78. Hill, M.A., *Cardiac MR imaging genotoxicity?* Eur Heart J, 2018. **39**(4): p. 313-315.

79. Glans, A., J. Wilén, and L. Lindgren, *Maintaining image quality while reducing acoustic noise and switched gradient field exposure during lumbar MRI*. J Magn Reson Imaging, 2021. doi: 10.1002/jmri.27527.

80. Wilén, J., J. Hauksson, and K. Hansson Mild, *Modification of pulse sequences reduces occupational exposure from MRI switched gradient fields: Preliminary results*. Bioelectromagnetics, 2010. **31**(1): p. 85-87.

81. Kheifets, L., et al., *The sensitivity of children to electromagnetic fields*. Pediatrics, 2005. **116**(2): p. e303-e313.